ACS EARTH AND SPACE CHEMISTRY

http://pubs.acs.org/journal/aesccq

Article

Kinetics and Products of Heterogeneous Hydroxyl Radical Oxidation of Isoprene Epoxydiol-Derived Secondary Organic Aerosol

Jin Yan, Yue Zhang, Yuzhi Chen, N. Cazimir Armstrong, Nicolas A. Buchenau, Ziying Lei, Yao Xiao, Zhenfa Zhang, Andrew T. Lambe, Man Nin Chan, Barbara J. Turpin, Avram Gold, Andrew P. Ault,* and Jason D. Surratt*

Cite This: *ACS Earth Space Chem.* 2023, 7, 1916–1928

Read Online

ACCESS | Metrics & More | Article Recommendations | Supporting Information

ABSTRACT: Heterogeneous hydroxyl radical (•OH) oxidation is an important aging process for isoprene epoxydiol-derived secondary organic aerosol (IEPOX-SOA) that alters its chemical composition. It was recently demonstrated that heterogeneous •OH oxidation can age single-component particulate methyltetrol sulfates (MTSs), causing ∼55% of the SOA mass loss. However, our most recent study of freshly generated IEPOX-SOA particulate mixtures suggests that the lifetime of the complete IEPOX-SOA mixture against heterogeneous •OH oxidation can be prolonged through the fragmentation of higher-order oligomers. Published studies suggest that the heterogeneous •OH oxidation of IEPOX-SOA could affect the organic atmospheric aerosol budget at varying rates, depending on aerosol chemical composition. However, heterogeneous •OH oxidation kinetics for the full IEPOX-SOA particulate mixture have not been reported. Here, we exposed freshly generated IEPOX-SOA particles to heterogeneous oxidation by •OH under humid conditions (relative humidity ∼57%) for 0−15 atmospheric-equivalent days of aging and derived an effective heterogeneous •OH rate coefficient (k_{OH}) of 2.64 ± 0.4 × 10^{-13} cm^3 $molecules^{-1}$ s^{-1}. While ∼44% of particulate organic mass of nonoxidized IEPOX-SOA was consumed over the entire 15 day aging period, only <7% was consumed during the initial 10 aging days. By molecular-level chemical analysis, we determined oligomers were consumed at a faster rate (by a factor of 2−4) than monomers. Analysis of aerosol physicochemical properties shows that IEPOX-SOA has a core−shell morphology, and the shell becomes thinner with •OH oxidation. In summary, this study demonstrates that heterogeneous •OH oxidation of IEPOX-SOA particles is a dynamic process in which aerosol chemical composition and physicochemical properties play important roles.

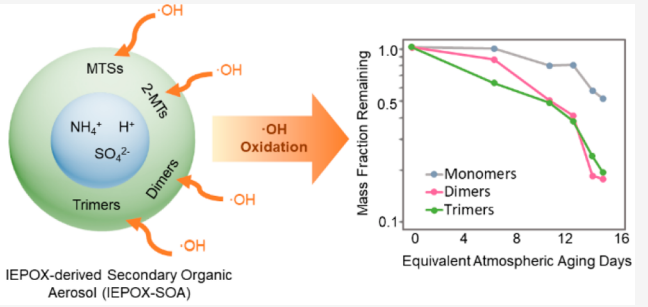

KEYWORDS: *IEPOX-SOA, multiphase chemistry, heterogeneous reactions, oligomers, organosulfates*

INTRODUCTION

Isoprene (2-methyl-1,3-butadiene) is the most abundant nonmethane volatile organic compound (VOC) emitted annually into Earth's atmosphere.[1−3] Its emissions are predicted to increase in a changing climate.[4−7] Under low-nitric oxide (NO) conditions, hydroxyl radical (•OH)-initiated oxidation of isoprene produces large quantities (>70% yield) of isoprene hydroxyhydroperoxides (ISOPOOHs), which subsequently oxidize in the gas phase to form isoprene epoxydiols (IEPOXs) (∼75% yield).[8−10] Gas-phase IEPOX can then react with inorganic sulfate aerosol particles through acid-catalyzed multiphase chemistry (reactive uptake) to form substantial amounts of secondary organic aerosol (SOA) within atmospheric fine particulate matter ($PM_{2.5}$).[11−15] The IEPOX-derived SOA (IEPOX-SOA) consists predominantly of 2-methyltetrols (2-MTs, $C_5H_{12}O_4$), methyltetrol sulfates (MTSs, $C_5H_{12}O_7S$), MTS-derived dimers ($C_{10}H_{22}O_{10}S$), 2MT-derived dimers ($C_{10}H_{22}O_7$), and higher-order sulfated and nonsulfated oligomers,[16−20] as well as semivolatile $C_5H_{10}O_3$ compounds that were recently identified as 3-methyltetrahydrofuran-2,4-diols and 3-methylenebutane-1,2,4-triol.[21] IEPOX-SOA can contribute 17−36% of submicrometer organic aerosol mass in the Southeastern United States (SE US) and Amazon rainforest,[22] with fine particulate MTSs and 2-MTs being dominant SOA constituents.[23−26] Prior studies illustrate that IEPOX-SOA particles are ubiquitous in ambient air and affect both climate[27,28] and human health,[29−31] underlining the need to investigate the atmospheric chemical fate of IEPOX-SOA.

Received: March 20, 2023
Revised: August 10, 2023
Accepted: September 6, 2023
Published: September 22, 2023

https://doi.org/10.1021/acsearthspacechem.3c00073
ACS Earth Space Chem. 2023, 7, 1916−1928

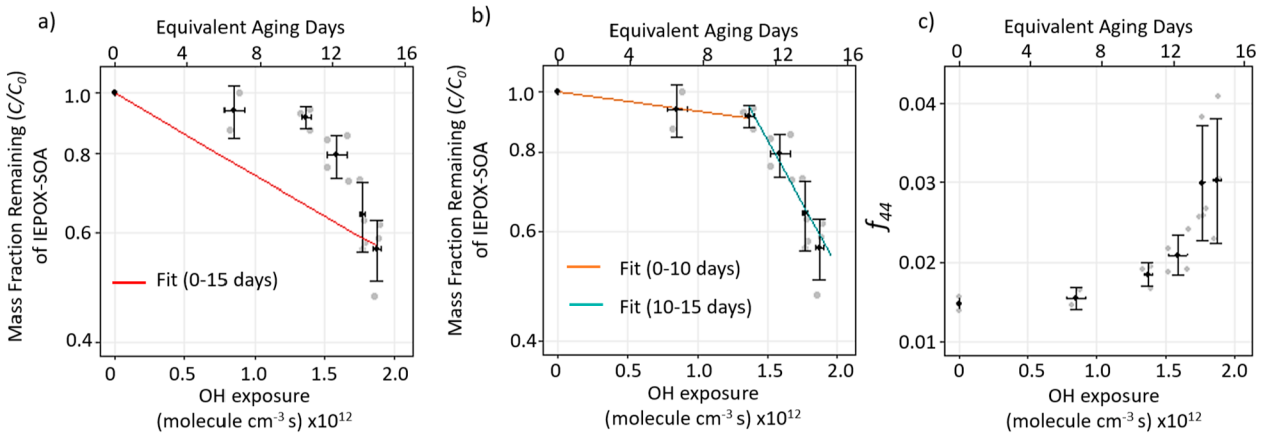

Figure 1. ACSM measured decay of total IEPOX-SOA particle mass with •OH exposures, fitted for: (a) the entire aging period (0−15 days); (b) low (0−10 days) and high (10−15 days) •OH exposure levels. The oxidation state is shown in (c), as indicated by the ACSM-derived f_{44}. The top *x*-axis shown in each panel is the equivalent photochemical age, assuming a 24 h averaged •OH concentration of 1.5×10^6 molecules cm^{-3}. Each gray dot represents a value obtained from one experiment at each specific •OH exposure. Black dots in each panel show the average values, and one standard deviation error bars from all conducted experiments are displayed.

Several studies[32−34] have used oxidation flow reactors (OFRs) to examine the heterogeneous •OH oxidation as a potential chemical sink of IEPOX-SOA particles under low-NO conditions and reported similar rate coefficients (k_{OH}) of 4.9 and 4.74×10^{-13} cm^3 molecule^{-1} s^{-1} for 2-MTSs[32] and 3-MTSs,[33] respectively. However, heterogeneous oxidation kinetics for the whole ambient IEPOX-SOA particle mixture, which may have a core−shell morphology, likely differs from that of single-component aerosols.[15] Only one chamber study has directly examined the chemical composition changes of suspended IEPOX-SOA particles against heterogeneous •OH oxidation and proposed that the decomposition of oligomers can regenerate low-volatility products that extend the apparent lifetime of IEPOX-SOA.[35] A viscous organic coating[15,27,36] also affects the reactive uptake of •OH.[37,38] Furthermore, a field study,[34] in which $PM_{2.5}$ collected in the SE US and Amazon rainforest was oxidized by •OH in an OFR, separated IEPOX-SOA particles from other ambient organic aerosol types using a positive matrix factorization (PMF) method and reported a k_{OH} value of ∼4 ± 2 × 10^{-13} cm^3 molecule^{-1} s^{-1}. Most atmospheric chemistry models still assume that IEPOX-SOA particles remain unreactive toward heterogeneous •OH oxidation.[39,40] To our knowledge, only one study incorporated heterogeneous •OH oxidation of IEPOX-SOA particles into the Community Earth System Model (CESM2.1.0); addition of this chemical aging process did not significantly change the SOA yield, but the other physicochemical properties were not examined.[41]

In addition, no laboratory study has reported the heterogeneous •OH oxidation kinetics of IEPOX-SOA particles, posing challenges in predicting the potential aerosol air quality and climate effects. Many organosulfates (OSs) identified in laboratory-aged particulate 2-MTSs[32] have been detected in cloudwater,[42,43] ice-nucleating particles,[44] rainwater,[45] and hailstone samples[45] collected from forested areas. In this study, we systematically examined the heterogeneous •OH oxidation of freshly generated IEPOX-SOA particles in a controlled laboratory environment at ∼57% relative humidity (RH), which is a typical daytime RH during the summer in the SE US.[46] Heterogeneous •OH oxidation kinetics were derived for both the bulk particle mixture and specific particulate species. The morphology of the IEPOX-SOA particles was also analyzed at different •OH exposures.

MATERIALS AND METHODS

Detailed experimental procedures are provided in Figure S1 and Section S1. IEPOX-SOA particles were generated by reacting acidified ammonium sulfate (AAS) aerosol particles (atomization of an AAS solution acidified to pH 1.6 with H_2SO_4) with gas-phase *trans*-*β*-IEPOX in two entrained gas-aerosol flow reactors under dark conditions. *Cis*- and *trans*-*β*-IEPOX account for >97% of IEPOX isomers formed from atmospheric oxidation of isoprene under low-NO conditions, and *trans*-*β*-IEPOX generates twice as much SOA as *cis*-*β*-IEPOX,[47] making it the most abundant contributor to IEPOX-SOA in the atmosphere. *Trans*-*β*-IEPOX was synthesized in-house as previously described in detail.[48] IEPOX-SOA particles were freshly generated in the entrained gas-aerosol flow reactors, chemically aged in a potential aerosol mass (PAM) OFR (Aerodyne Research, Inc.) after gas-phase IEPOX was removed using a carbon strip denuder (Sunset Lab, Inc.) upstream of the OFR inlet to avoid gas-phase reactions between IEPOX and •OH. The •OH exposures and UV lamp flux inside the OFR were estimated using a photochemical box model based on residence time, temperature, RH, and ozone concentration with and without internal UV illumination.[49−51] The detailed procedures for the •OH exposure estimation and discussion of the model performance are included in Section S2. Varying •OH exposures (0−1.9×10^{12} molecules cm^{-3} s), equivalent to 0−15 days of atmospheric •OH exposure assuming an ambient •OH concentration of 1.5×10^6 molecules cm^{-3},[52] were achieved by varying the ozone (O_3) mixing ratio from 0 to 6500 ppbv at an average UV (254 nm) photon flux of 1.25×10^{15} photons cm^{-2} s^{-1}. In this study, the term "nonoxidized IEPOX-SOA" refers to freshly generated IEPOX-SOA exposed to only UV photon flux. Two to four experiments were repeated at each •OH exposure level, and their conditions are summarized in Table S1.

Aged IEPOX-SOA particles exiting the OFR were sampled by a scanning electrical mobility spectrometer (SEMS, Brechtel Inc., Model 2002) and an aerosol chemical speciation monitor (ACSM, Aerodyne Research, Inc.) for real-time aerosol size

https://doi.org/10.1021/acsearthspacechem.3c00073
ACS Earth Space Chem. 2023, 7, 1916−1928

distribution and chemical composition measurements, respectively, as well as collected onto 47 mm Teflon filters (2-μm pore size, PALL Corp) for offline chemical analyses using hydrophilic interaction liquid chromatography interfaced to an electrospray ionization high-resolution quadrupole time-of-flight mass spectrometer operated in the negative ion mode (HILIC/(−)ESI-HR-QTOFMS) (details in Section S3).[53] Authentic standards listed in Table S2 were used to quantify specific IEPOX-SOA species (details in Section S4). Aerosol morphology and composition were probed using atomic force microscopy coupled with photothermal infrared spectroscopy (AFM-PTIR, Bruker) (details in Section S5).[54,55] No unexpected or unusually high safety hazards were encountered during our experiments and filter processing procedures.

RESULTS AND DISCUSSION

Estimation of Heterogeneous •OH Oxidation Rate Constant (k_{OH}). Based on ACSM data, the organic mass remaining in IEPOX-SOA particles can be calculated as particulate organic concentration in aged IEPOX-SOA aerosol particles at each •OH exposure level (C) normalized to that in nonoxidized IEPOX-SOA aerosol particles (C_0). The mass decay of IEPOX-SOA with •OH oxidation (Figure 1) can be fitted with an exponential function (eq 1) to derive the heterogeneous oxidation second-order rate constant k_{OH}.

$$\ln(C/C_0) = -k_{OH}([OH] \times t) \quad (1)$$

where $[OH] \times t$ is •OH exposure (molecules cm^{-3} s), [OH] is 24 h-averaged ambient •OH concentration, 1.5×10^6 molecules cm^{-3},[52] and t is the equivalent aging time of IEPOX-SOA particles in ambient air, calculated as •OH exposure divided by [OH]. k_{OH} is the slope of fitted line, as the y-axis (on log scale) is $\ln(C/C_0)$ and the x-axis is •OH exposure ($[OH] \times t$).

k_{OH} values obtained in this study (Table S3) include: (1) $k_{OH,0-15days}$ for the whole aging period, equivalent to 0−15 aging days; (2) $k_{OH,<10days}$ for low OH exposure period, equivalent to 0−10 aging days; (3) $k_{OH,>10days}$ for high •OH exposure period, equivalent to 10−15 aging days. The fitting protocols are shown separately in Figure 1a,b for clarity.

As shown in Figure 1a,b, IEPOX-SOA decreased by <7% under low •OH exposures of 0−1.4×10^{12} molecules cm^{-3} s, which is equivalent to 0−10 days of atmospheric •OH exposure. At higher •OH exposures ($1.4-1.9 \times 10^{12}$ molecules cm^{-3} s), or 10−15 equivalent aging days, about 44% of organic mass in freshly generated IEPOX-SOA particles is consumed. The fraction of the ion detected by the ACSM at m/z 44 (most likely CO_2^+) to total measured ACSM organics (f_{44}), a marker for the oxidation state of oxidized organic aerosols (OOA),[56−58] doubled from 0.015 to 0.03 as shown in Figure 1c. f_{44} reported here for oxidized IEPOX-SOA (0.03) is smaller than that for ambient OOA (>0.05)[59] and IEPOX-SOA factor from PMF analysis (0.12−0.14 in the Southern Great Plains),[60] possibly due to the higher organic mass loading of laboratory-generated IEPOX-SOA in this study. A previous study observed a decrease of f_{44} with increasing OA mass loadings, likely due to the more effective partitioning of less oxidized and more volatile species into the aerosol phase at higher OA loadings.[61] In summary, as indicated by the mass decay and corresponding f_{44} increase, IEPOX-SOA particles begin to decay rapidly after 10 equivalent aging days. This may be due to the regeneration of monomers in IEPOX-SOA through fragmentation of oligomers during the heterogeneous •OH oxidation process.[35] Thus, the definition of k_{OH} determined in this study should be distinguished from the conventional understanding of k_{OH} generally reported for pure OA aerosols. In this study, k_{OH} can be redefined as the "effective heterogeneous •OH oxidation rate constant", describing how fast the combined process (regeneration of monomers from oligomer oxidation + oxidation of monomers to volatile fragments) occurs. Discussion on the definition of the k_{OH} definition is in Section S6.

Several factors may introduce uncertainties in deriving k_{OH}: (1) the deviation of each specific •OH exposure and the aerosol mass fraction remaining from the averaged values that were used to derive k_{OH} across repeated experiments; (2) the collection efficiency (CE) and relative ionization efficiency (RIE) of ACSM measurements; and (3) photolysis and ozonolysis reactions of IEPOX-SOA. We observed that the decay trend of the SEMS-measured total volume concentration agrees very well with that for ACSM-measured total particle mass (Figure S5), suggesting that CE and RIE do not change with •OH oxidation in this study. Detailed discussions are included in Section S7. Photolysis and ozonolysis reactions were also assessed inside the PAM-OFR. We observed a 3% increase and 7% decrease of IEPOX-SOA mass in UV-only and O_3-only control experiments, respectively (Figure S6). Since all oxidation experiments were conducted at near constant UV flux with varying O_3 concentration, it is reasonable to conclude that the IEPOX-SOA mass changes from photolysis remain constant, while from ozonolysis they may vary at different •OH exposure levels and could affect the derived oxidation kinetics. We modeled the mass decay caused by ozonolysis (Figure S7) and found that ozonolysis caused a negligible change in the derived k_{OH} values (detailed discussion is included in Section S8).

In conclusion, the uncertainties in k_{OH} from CE and RIE changes in the ACSM and from photolysis and ozonolysis of IEPOX-SOA are negligible in this study. The uncertainty in k_{OH} was estimated using a Monte Carlo simulation, propagated from uncertainties in •OH exposure calculation (x-axis error bar) and mass fraction remaining (y-axis error bar), assuming normal distributions for each parameter. Detailed procedures for estimating k_{OH} uncertainty are provided in Section S9 and shown in Figure S8.

Estimation of Reactive Uptake Coefficient of •OH (γ_{OH}). The effective reactive uptake coefficient of •OH (γ_{OH}) for IEPOX-SOA particles in the PAM-OFR can be estimated using k_{OH} following eq 2:[62]

$$\gamma_{OH} = \frac{4k_{OH}V\rho_0 N_A}{\bar{c}S \times MW} \quad (2)$$

where k_{OH} is the effective heterogeneous •OH oxidation rate coefficient of IEPOX-SOA derived from this study (Table S3). V and S are the mean volume and surface areas of IEPOX-SOA from the SEMS measurements, respectively. The V/S ratio is calculated to be 69.6 ± 3.7 nm. N_A is Avogadro's number (6.02×10^{23} molecules mol^{-1}); $\bar{c}$ is the average molecular speed of •OH, 604 m s^{-1} at 293 K. MW is the molar mass of IEPOX-SOA, calculated as the average molecular weight of all IEPOX-SOA species quantified in HILIC/(−)ESI-HR-QTOFMS (Table S4) using eq 3 below:

$$MW = \left(\sum_i n_i MW_i\right) / \sum_i n_i \quad (3)$$

https://doi.org/10.1021/acsearthspacechem.3c00073
ACS Earth Space Chem. 2023, 7, 1916−1928

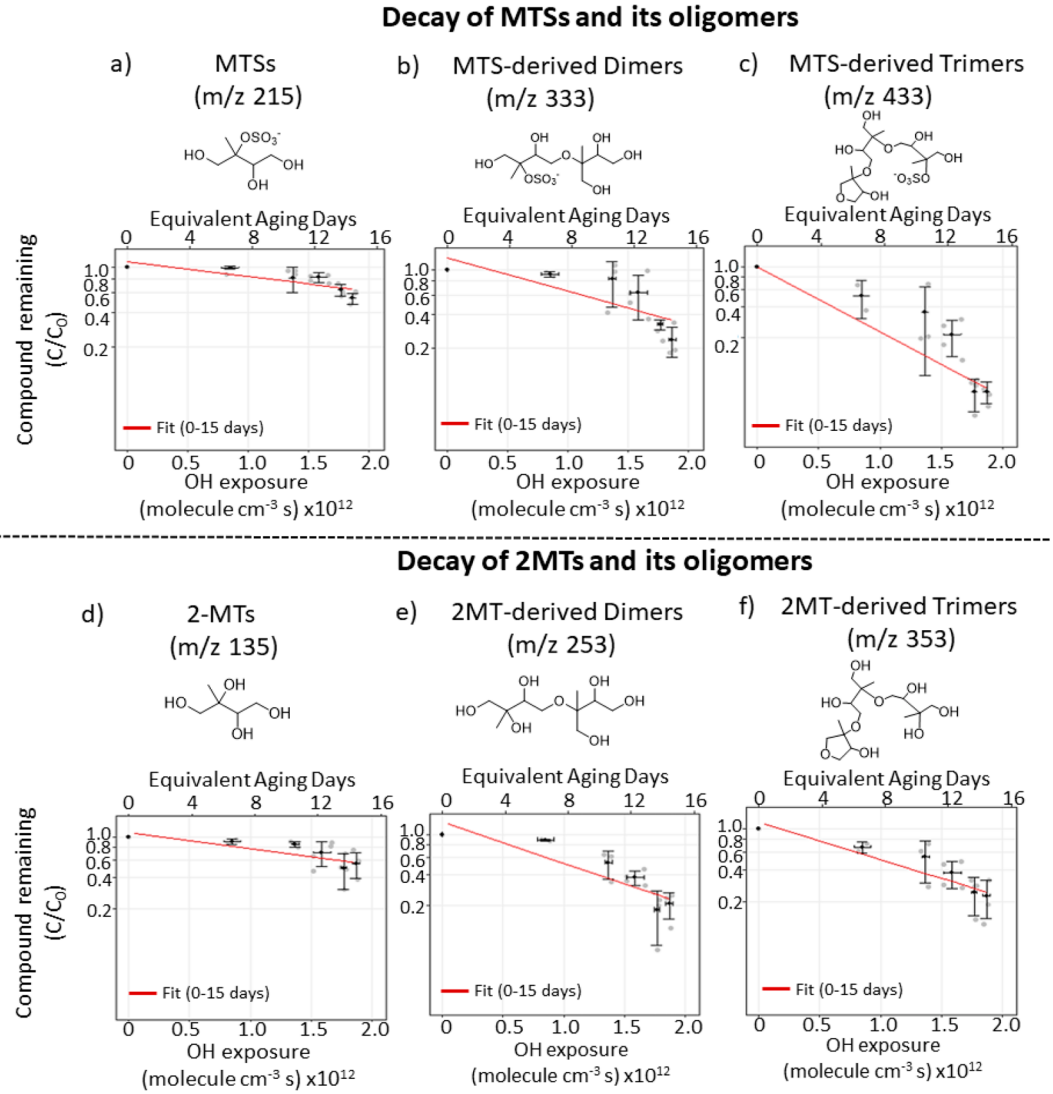

Figure 2. Decay of freshly generated IEPOX-SOA particle constituents with exposure to gas-phase •OH. Nonoxidized IEPOX-SOA particle constituents are identified as $[M - H]^-$ ions at m/z 215 ($C_5H_{11}O_7S^-$), 333 ($C_{10}H_{21}O_{10}S^-$), 433 ($C_{15}H_{29}O_{12}S^-$), 135 ($C_5H_{11}O_4^-$), 253 ($C_{10}H_{21}O_7^-$), and 353 ($C_{15}H_{29}O_9^-$), corresponding to (a) MTSs, (b) MTS-derived dimers, (c) dehydration product of MTS-derived trimers, (d) 2-MTs, (e) 2-MT-derived dimers, and (f) dehydration product of 2-MT-derived trimers; one possible isomeric structure is shown above each graph.

where MW_i is the molecular weight and n_i is number of moles for species i. MW of IEPOX-SOA is estimated to be 198.9 ± 5.8 g mol^{-1} across all •OH exposures from repeated experiments. The ambient IEPOX-SOA has a much larger MW of 270 g mol^{-1}, as they are oligomer-dominant based on volatility measurements using a thermal denuder.[34] The laboratory-generated IEPOX-SOA in this study has a much lower organic content and, thus, less oligomeric fraction, compared to ambient IEPOX-SOA (Figure S9), which may be a result of the short reaction times (~16 min) inherent to the entrained gas-aerosol flow reactors.

ρ_0 is the mass density for IEPOX-SOA, which is calculated as the total particle mass concentration measured by ACSM normalized to the total particle volume concentration measured by SEMS and is estimated to be 1.6 ± 0.1 g cm^{-3} within the range of 1.5 ± 0.5 g cm^{-3} for ambient IEPOX-SOA[34] and slightly higher than that of 1.48 ± 0.02 g cm^{-3} estimated using single particle mass spectrometry.[63] The uncertainty of γ_{OH} was estimated by Monte Carlo simulation, propagated from errors in each parameter in eq 2, assuming normal distribution for each parameter.

The k_{OH} and γ_{OH} values reported in this study are compared to previously reported values for different ambient and laboratory OA types (Table S4). $k_{OH,0-15days}$ (2.6 ± 0.4 × 10^{-13} cm^3 molecule^{-1} s^{-1}) and $\gamma_{OH,0-15\ days}$ (0.6 ± 0.1) derived for an IEPOX-SOA bulk mixture in this study are within the range of k_{OH} (0.44−7.6 × 10^{-13} cm^3 molecule^{-1} s^{-1}) and γ_{OH} (0.07−1.65) values reported for ambient IEPOX-SOA particles,[34] MTSs,[32,33] levoglucosan,[64,65] and other highly oxidized organic species (e.g., tartaric acid).[64,66,67]

Estimation of Lifetime of IEPOX-SOA against •OH Oxidation (τ_{OH}). As shown in eq 4, the lifetimes of IEPOX-SOA against •OH oxidation (τ_{OH}) in different world regions were estimated using γ_{OH} derived for the IEPOX-SOA particles (0.6 ± 0.1) and using ambient aerosol parameters reported from prior field studies, as listed in Table S5.

https://doi.org/10.1021/acsearthspacechem.3c00073
ACS Earth Space Chem. 2023, 7, 1916−1928

$$\tau_{OH} = \frac{4V\rho N_A}{S\bar{c} \times MW \times \gamma_{OH}[OH]} = \frac{2d_{surf}\rho N_A}{3\bar{c} \times MW \times \gamma_{OH}[OH]} \quad (4)$$

where V and S are the volume and surface areas of ambient aerosols, ρ is the mass density of ambient aerosol, MW is the molar mass of ambient IEPOX-SOA, which is assumed to be 270 g/mol,[34] N_A is Avogadro's constant, and $\bar{c}$ is the average molecular speed of •OH (604 m s^{-1}) at 293 K. When assuming IEPOX-SOA compounds are uniformly mixed with other species in ambient aerosols, the V/S ratio of IEPOX-SOA can be estimated as the surface-weighted diameter of ambient aerosol (d_{surf})/6.

In forested areas with lower •OH concentration, such as the SE US (0.6×10^6 molecules cm^{-3}) and central Amazonia (0.3×10^6 molecules cm^{-3}),[8,34] ambient aerosols are estimated to have τ_{OH} of ∼51 days in the SE US and ∼118 days in central Amazonia, potentially enabling long distance transport of IEPOX-SOA. τ_{OH} for IEPOX-SOA may change drastically as the once pristine Amazon is affected by increasing biomass burning and anthropogenic emissions. A recent study used multiwavelength polarization Raman lidar to track the aerosol properties in biomass burning plumes in the Amazon forest; they observed that the aerosol effective radius (or surface-weighted radius) of fresh smoke particles increases from 130 to 300 nm after 1−2 days of transport,[68] extending τ_{OH} of IEPOX-SOA as calculated by eq 4. Another study observed that noon-time •OH concentration increases by at least 250% with increasing NO_x levels,[69] shortening the τ_{OH} of IEPOX-SOA. In polluted urban areas, such as Los Angeles and New England, US,[70,71] and Guangzhou and Beijing, China,[72,73] elevated •OH concentrations have been observed ($3-21 \times 10^6$ molecules cm^{-3}). The τ_{OH} values of IEPOX-SOA under heavily polluted urban air environments during summer in Beijing and Guangzhou are estimated to be only ∼2 to 3 days. Overall, the lifetime of ambient IEPOX-SOA against •OH oxidation varies between 2 and 118 days from polluted urban cities to pristine forested areas. Detailed atmospheric-relevant parameters from multiple field studies used to calculate τ_{OH} are listed in Section S10.

At the global average atmospheric •OH concentration of 1.5×10^6 molecules cm^{-3}, the average atmospheric lifetime of IEPOX-SOA is estimated to be ∼21 ± 5 days (based on aerosol parameters averaged across all ambient studies listed in Table S5). As discussed above, the higher •OH concentrations in polluted air masses influenced by anthropogenic interactions may reduce the atmospheric lifetime. At higher •OH exposure levels, $\gamma_{OH,>10days}$ derived for IEPOX-SOA bulk mixtures is calculated to be 2.2 ± 0.6. The average oxidation lifetime of IEPOX-SOA is reduced with application of the $\gamma_{OH,>10days}$ value (∼6 ± 1 days), putting it in a similar range as the aerosol wet deposition lifetime (6.6−9.0 days),[74] and shorter than the lifetime of accumulation mode sulfate aerosol (2 weeks),[75] indicating that heterogeneous •OH oxidation could be a competitive sink for IEPOX-SOA under the atmospheric scenarios discussed above. These results suggest that IEPOX-SOA lifetimes may change drastically during atmospheric transport, and utilizing a single k_{OH} value to represent heterogeneous •OH oxidation kinetics in atmospheric models may be insufficient.

Heterogeneous •OH Oxidation Kinetics of Oligomers and Monomers. MTSs, 2-MTs, and their dimers and trimers detected by HILIC/(−)ESI-HR-QTOFMS account for ∼90% of total mass measured in nonoxidized IEPOX-SOA (Figure S10). Dimers and trimers are derived from acid-catalyzed particle-phase reactions of IEPOX with MTSs and 2MTs (Scheme S1). These nonoxidized IEPOX-SOA species in this study show retention times similar to ambient $PM_{2.5}$ samples (Figure S11). The oxidized species contribute ∼7.3% of nonoxidized IEPOX-SOA, likely due to organic contaminants off-gassing from the OFR inner wall. The remaining 4.5% of the total SOA mass was not quantified by HILIC/(−)ESI-HR-QTOFMS. The use of proxy standards due to the unavailability of authentic standards for oligomers and oxidized products could contribute to the inaccurate quantification of IEPOX-SOA.

The nonoxidized IEPOX-SOA constituents exhibit varying degrees of consumption by heterogeneous •OH oxidation. We derived the compound-based k_{OH} values based on the mass decay trend of specific IEPOX-SOA species for the entire aging period (0−15 days), as shown in Figure 2, and for low (0−10 days) and high (10−15 days) •OH exposure periods, as shown in Figure S12. Compared to C_5-monomers (MTSs and 2-MTs), the C_{10}/C_{15}-oligomers (i.e., MTS-derived and 2-MT-derived dimers and trimers) show much faster decay: ∼78−96% of oligomer mass depleted after 15 days ($k_{OH,0-15days}$ = $7.08-14.92 \times 10^{-13}$ cm^3 $molecule^{-1}$ s^{-1}). The $k_{OH,>10\ days}$ values for MTS-derived dimers, 2-MT-derived dimers and trimers ($18.23-39.40 \times 10^{-13}$ cm^3 $molecule^{-1}$ s^{-1}) are on the same scale as the photooxidation rates of different C_{16-19}-dimers in α-pinene-derived SOA (21.6×10^{-13} cm^3 $molecule^{-1}$ s^{-1}).[76]

Three factors may contribute to the faster decay rate of oligomers compared to monomers: (1) The longer oligomer carbon chains increase the probability of hydrogen atom abstraction by •OH with subsequent C−C bond scission. (2) Consumption of monomers by heterogeneous •OH oxidation may be masked by their regeneration through oxidative fragmentation of oligomers. We have reported that the MTS-trimers decompose by heterogeneous •OH oxidation to regenerate particulate MTSs and 2-MT-dimers (Scheme S2).[35] (3) Sulfated oligomers may be surface-active providing greater access to gas-phase •OH. Highly surface-active oligomeric species have been reported near the air−water interface of an aqueous pyruvic acid mixture using vibrational sum frequency spectroscopy (VSFS).[77] Further experiments are needed to verify these hypotheses.

Physicochemical Properties of IEPOX-SOA Particles. In this study, we observed that the heterogeneous •OH oxidation rate of IEPOX-SOA particles changes as a function of •OH exposure, which differs from the constant oxidation rate reported for single-component liquid-like OA types, such as pure 2-MTS and 3-MTS.[32,33] Similar slow oxidation rates at low •OH exposures have been observed in heterogeneous •OH oxidation of atmospheric IEPOX-SOA.[34] In addition, the $k_{OH,>10days}$ values reported here are higher compared to previously reported kinetic values for single-component 2-MTS and 3-MTS particles.[32,33] Analogous behavior involving faster heterogeneous •OH reaction rates have also been reported for squalane-coated (1−50 nm thickness) ammonium sulfate aerosol compared to pure squalene aerosol, with the reaction rate being linearly dependent on organic surface area-to-volume ratio (thicker organic coating, slower reaction).[78] Thus, we suspect that the changing oxidation rates with •OH exposure observed for IEPOX-SOA particles may be related to

https://doi.org/10.1021/acsearthspacechem.3c00073
ACS Earth Space Chem. 2023, 7, 1916−1928

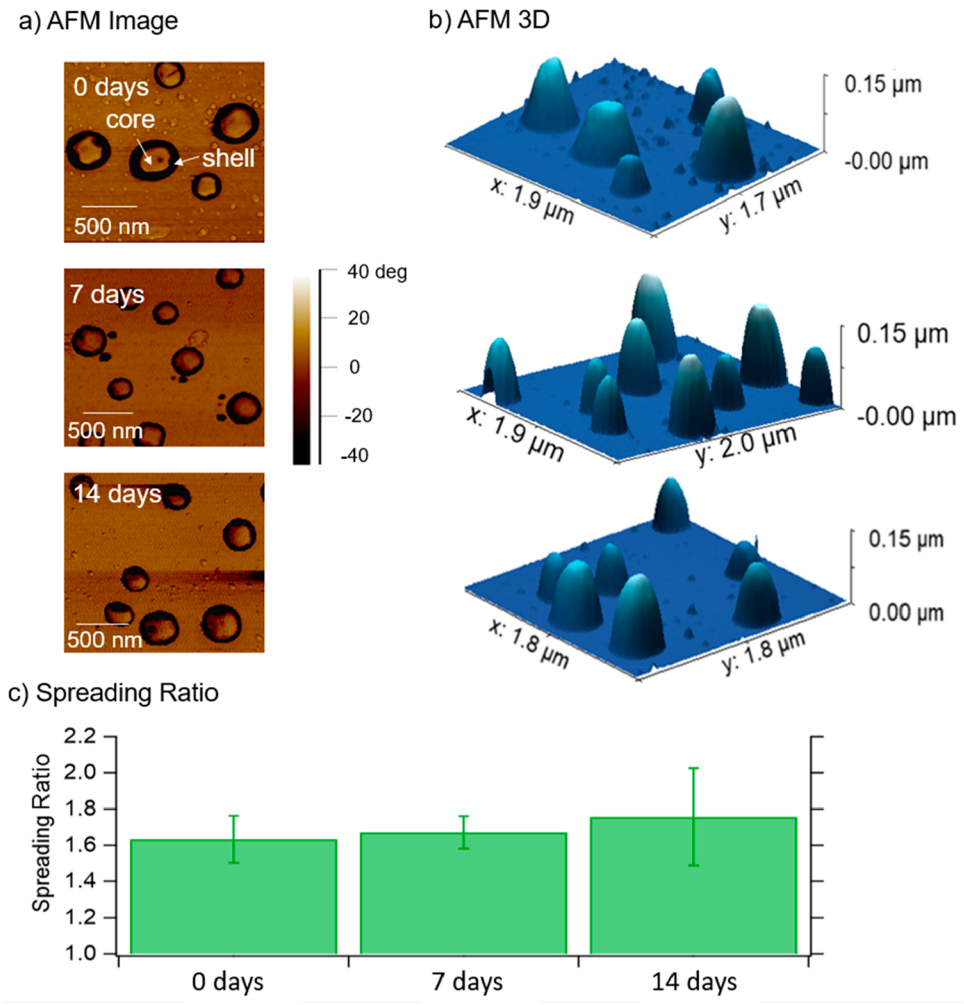

Figure 3. IEPOX-SOA particle morphology and viscosity at 0, 7, and 14 equiv days of •OH exposure characterized: (a) AFM-derived phase images; (b) AFM-derived 3D images; (c) spreading ratios of IEPOX-SOA particles.

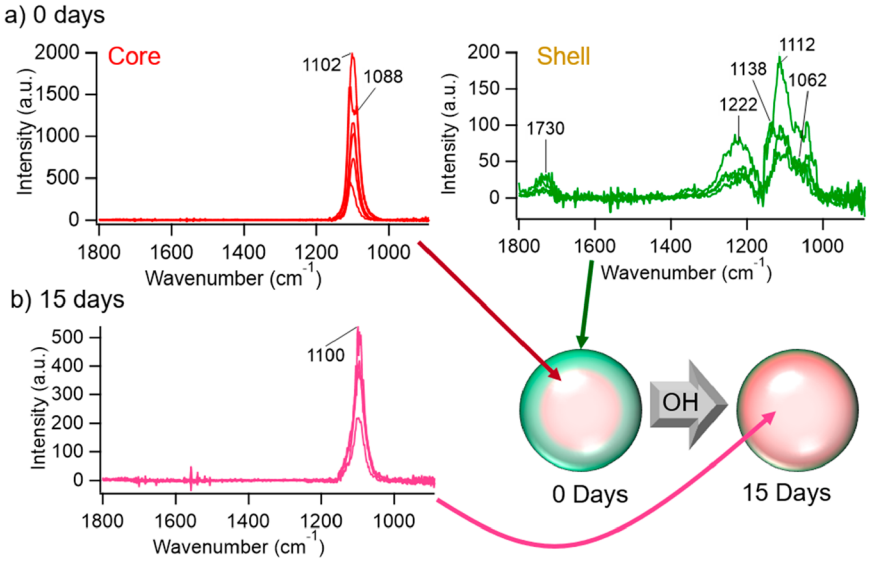

Figure 4. (a) PTIR spectra of individual nonoxidized or 0 day-aged IEPOX-SOA particles; (b) PTIR spectra of IEPOX-SOA particles aged for 15 days by heterogeneous •OH oxidation. Red color represents the PTIR spectra of the IEPOX-SOA particle core, and green color represents the PTIR spectra of IEPOX-SOA particle shell. The PTIR spectra of the IEPOX-SOA particle shell is not shown for 15 day-aged IEPOX-SOA, as the signal intensity is too low due to excessive OA removed by heterogeneous •OH oxidation.

https://doi.org/10.1021/acsearthspacechem.3c00073
ACS Earth Space Chem. 2023, 7, 1916−1928

the changes in their corresponding aerosol physicochemical properties that result from their oligomeric contents.

The AFM-derived phase image (Figure 3a) shows that nonoxidized IEPOX-SOA particles have a core−shell morphology. The shell thickness of IEPOX-SOA could be obtained using the geometric mean diameters (GMDs) of IEPOX-SOA and AAS seed aerosols measured by SEMS (Figure S13): nonoxidized IEPOX-SOA particles have a GMD of 114 nm and a shell thickness of 11 nm with the shell thickness decreasing to 2 nm after 15 equivalent aging days. The shell in the AFM-derived phase image decreases in thickness as a function of oxidation days (Figure 3a), providing independent support for the SEMS-observed decrease in thickness.

The AFM-derived height images of IEPOX-SOA (Figure 3b) were used to calculate the spreading ratios of individual particles, which has been used in prior studies to distinguish changes in viscosity.[79−81] At least 98 particles at each $^{\bullet}$OH exposure level are selected to obtain the average $\pm 2\sigma$ from Gaussian fit as shown in Figure 3c. The spreading ratio increased slightly from 1.7 ± 0.1 to 1.8 ± 0.3 during 0−14 aging days, suggesting that the aerosol viscosity change is not statistically significant. Rather than aerosol viscosity, the driving factors for faster heterogeneous oxidation we observed at higher $^{\bullet}$OH exposures may be the coating thickness and oligomer reactivity.

AFM-PTIR analysis in Figure 4 demonstrates that the core of IEPOX-SOA is dominated by inorganic sulfate, while the shell is organic in nature consisting of IEPOX-SOA. For the particle core, the vibrational mode at ∼1102 cm^{-1} is assigned to inorganic SO_4^{2-} (antisymmetric stretch).[82] For the shell, the modes detected at 1062 and 1112 cm^{-1} are organic in nature and are likely attributable to C−O stretching, while the mode at 1732 cm^{-1} indicates the presence of carbonyls (C═O bond).[83]

Since the only vibrational mode observed in the core is for inorganic SO_4^{2-} for both nonoxidized and oxidized IEPOX-SOA, the heterogeneous $^{\bullet}$OH oxidation is likely occurring in the aerosol shell where IEPOX-SOA predominates. We further suspect that heterogeneous $^{\bullet}$OH oxidation of IEPOX-SOA may only occur at the air−particle interface because the reactive-diffusive length of $^{\bullet}$OH in IEPOX-SOA may be shorter than that measured in squalane-derived OA (∼1.4 nm),[38] as viscosity of IEPOX-SOA coating (10^8−10^9 mPa·s) is orders of magnitude higher than that of squalane (36.1 mPa·s).[84] By 15 days, the organic material is no longer observable within the shell because shell thickness has been reduced to 2.3 nm (as measured by SEMS), which is a point where the concentration of IEPOX-SOA is below the sensitivity of the AFM-PTIR instrument.

Oxidation Products of IEPOX-SOA Particles. Scheme S3a illustrates a general mechanism for heterogeneous $^{\bullet}$OH oxidation under low-NO atmospheric conditions. Heterogeneous $^{\bullet}$OH oxidation is initiated by hydrogen atom (H) abstraction by $^{\bullet}$OH, followed by the addition of O_2 to form a peroxyl radical ($RO_2^{\bullet}$). Under low-NO atmospheric conditions, $RO_2^{\bullet}$ can cross react through the Russell[85] or Bennett−Summers[86] mechanisms to give an alcohol or carbonyl group at the abstraction site or form alkoxy radicals ($RO^{\bullet}$) followed by radical propagation,[87] fragmentation through β-scission,[88] and isomerization[89] pathways. The resulting first-generation particulate products consist of polyols and carbonyls including carboxylic acids, aldehydes, and ketones, which can cyclize to form 5-member ring structures such as lactones, cyclic hemiacetals, furans, and tetrahydrofurans (Scheme S3b). A full list of products detected in this study is shown in Table S6. In summary, after 15 equivalent days of aging by heterogeneous $^{\bullet}$OH oxidation, the oxidized multifunctional products listed in Table S6 contributed ∼13% of the total IEPOX-SOA mass. Nonoxidized (or regenerated) species including MTS, 2MT, and their oligomers comprised the majority (∼80%) of SOA mass (Figure S10).

As indicated above, inaccuracies in the quantification of aged IEPOX-SOA constituents as a result of using 2-MT and 2-MTS as surrogate standards highlight a critical need for synthesis of authentic heterogeneous oxidation reaction products. Volatile fragmentation products, such as formic acid, may have been formed in significant yields based on our proposed Schemes S2, S4, and S5; they were not measured in this study in either the particle or gas phases but should be a focus of future work, especially since recent bulk solution studies have also suggested their formation upon reaction with $^{\bullet}$OH.[90] The five most abundant oxidation products in aged IEPOX-SOA particles are OSs detected by HILIC/(−)ESI-HR-QTOFMS as deprotonated molecules at m/z 199 (2-methylglyceric sulfate, $C_4H_7O_7S^-$), 155 (glycolic acid sulfate, $C_2H_3O_6S^-$), 213 ($C_5H_9O_7S^-$), 211 ($C_5H_7O_7S^-$), and 229 ($C_5H_9O_8S^-$). Our laboratory has reported characterization of these ions tentatively by tandem mass spectrometry (MS/MS).[32,35,91] We have also characterized nonsulfated oxidation products from heterogeneous $^{\bullet}$OH oxidation of 2-MTs and 2-MT-derived oligomers. The most abundant $[M - H]^-$ ions observed by HILIC/(−)ESI-HR-QTOFMS appear at m/z 133 ($C_5H_9O_4^-$), 131 ($C_5H_7O_4^-$), 251 ($C_{10}H_{19}O_7^-$), and 147 ($C_5H_7O_5^-$). The proposed formation mechanisms for sulfated and nonsulfated particulate oxidation products are shown in Schemes S4 and S5, respectively. The levels of several oxidation products increase in aged IEPOX-SOA (Figures S14 and S15); they were also detected in ambient $PM_{2.5}$ samples from Look Rock and Raleigh, USA, Manaus, Brazil, and the Galápagos Islands, Ecuador (Figures S16 and S17). Ambient $PM_{2.5}$ samples contain multiple isomers, possibly formed by heterogeneous $^{\bullet}$OH oxidation of *cis*-β-IEPOX-SOA (∼33% of ambient IEPOX), which was not examined in the present study.[92] It should be noted that the reaction mechanisms proposed in this study are not well-established in the ambient atmosphere, especially since laboratory-generated aerosols are highly concentrated and thus possibly favor bimolecular $RO_2^{\bullet}$ + $RO_2^{\bullet}$ reactions to a greater extent than in ambient aerosols.[90]

■ CONCLUSIONS

This study demonstrated that the heterogeneous $^{\bullet}$OH oxidation of nonoxidized IEPOX-SOA particles is a dynamic process in which aerosol chemical composition and physicochemical properties play important roles. Oligomers in nonoxidized IEPOX-SOA particles decompose to form low-volatility oxidized fragments and to regenerate oxidized and nonoxidized monomers, slowing loss of organic SOA mass for an initial 10 day aging period. This process is supported by the more rapid mass decay (a factor of 2−4) of oligomers than monomers. The reaction of bulk IEPOX-SOA components with $^{\bullet}$OH is inhibited for an initial period of ∼10 days by the formation of an IEPOX-SOA coating. The thinning of the IEPOX-SOA coating thickness after 10 days likely contributes to an accelerated mass loss.

https://doi.org/10.1021/acsearthspacechem.3c00073
ACS Earth Space Chem. 2023, 7, 1916−1928

Concentrations of OSs at m/z 199, 155, 211, 213, and 229 previously reported in cloudwater, ice-nucleating particles, rainwater, and hailstone samples collected from forested areas[42−45] increased by a factor of 3 in laboratory-generated IEPOX-SOA particles over 15 equivalent aging days. The extensive generation of these multifunctional particulate OS products in aged IEPOX-SOA will affect aerosol acidity, volatility, phase, hygroscopicity, and light absorption[44,93−99] and play an important role in cloud formation.[44]

Overall, this study demonstrates that the complete IEPOX-SOA particle mixture behaves differently from single-component OA particles, and atmospheric chemistry models should therefore include SOA properties such as coating thickness and oligomer content to take into account the effects of heterogeneous •OH oxidation on IEPOX-SOA. This study also highlights the need for future investigations into the atmospheric aging of low-volatility IEPOX-SOA oligomers, as they appear to serve as a regeneration source of particulate monomers. Biogenic SOA is formed from many species of VOC precursors, including monoterpenes and isoprene, and thus, their resulting oligomer content, abundance, and physicochemical properties will differ.[100,101] Additional factors, such as temperature,[102] aerosol acidity,[103] and RH,[104] affect the oligomer content in IEPOX-SOA (and other SOA) and should also be considered in future atmospheric models that might consider chemical aging of particle-bound oligomers by heterogeneous •OH oxidation pathways.

This study intended to mimic the SE US environment. Compared to ambient IEPOX-SOA in the SE US,[34] our laboratory-generated IEPOX-SOAs have similar d_{surf} (418 versus 415 nm), slightly higher mass density (1.59 versus 1.46 g cm^{-3}), much less organic content (16.6% versus 66.9% in ambient aerosol), and lower MW (199 versus 270 g mol^{-1}). It is unclear how the differences in aerosol parameters could affect the oxidation kinetics. Future studies should be designed to mimic ambient organic aerosol mass fractions more closely using steady-state laboratory chambers that allow for longer reaction times.

■ ASSOCIATED CONTENT

Supporting Information

The Supporting Information is available free of charge at https://pubs.acs.org/doi/10.1021/acsearthspacechem.3c00073.

Section S1: Experiment setup and instrumentation; Section S2: Estimation of •OH exposures in PAM-OFR; Section S3: Filter preparation and off-line HILIC/(−)ESI-HR-QTOFMS analysis; Section S4: Authentic standards; Section S5: Atomic force microscopy coupled to photothermal infrared spectroscopy; Section S6: Discussion on definition of kOH in IEPOX-SOA System; Section S7: Collection efficiency and relative ionization efficiency of IEPOX-SOA in ACSM measurements; Section S8: Photolysis and ozonolysis of IEPOX-SOA in OFR; Section S9: Estimation of k_{OH} uncertainty using the Monte-Carlo method; Section S10: Information on ambient data used to calculate lifetime of IEPOX-SOA; Table S1: Summary of control and repeated experiments; Table S2: Authentic standards; Table S3: k_{OH} and γ_{OH} values; Table S4: Freshly generated IEPOX-SOA species detected in HILIC/(−)ESI-HR-QTOFMS analysis; Table S5: Ambient parameters used to estimate the oxidation lifetime of IEPOX-SOA; Table S6: Particulate oxidation products; Figure S1: Experimental setup; Figure S2: Time series of ozone concentrations; Figure S3: •OH exposures and UV lamp (254 nm) flux; Figure S4: Time series of ACSM-measured organics; Figure S5: ACSM-measured mass and SEMS-measured volume concentration decay; Figure S6: IEPOX-SOA mass change caused by ozonolysis and photolysis; Figure S7: modeled mass decay of IEPOX-SOA by ozonolysis; Figure S8: Monte Carlo Method to estimate the uncertainty in k_{OH} values; Figure S9: Organic content in laboratory-generated and ambient IEPOX-SOA; Figure S10: Contribution of identified oxidation products and unoxidized compounds to total organics; Figure S11: HILIC/(−)ESI-HR-QTOFMS extracted ion chromatograms of freshly-generated IEPOX-SOA constituents; Figure S12: Mass decay of freshly generated IEPOX-SOA particle constituents; Figure S13: Aerosol size distribution of IEPOX-SOA at varying •OH exposures; Figures S14 and S15: Formation of OS and non-OS oxidation products with •OH oxidation, respectively; Figures S16 and S17: HILIC/(−)ESI-HR-QTOFMS EICs of OS and non-OS oxidation; Scheme S1; Formation mechanism of freshly generated IEPOX-SOA constituents; Scheme S2: Regeneration mechanisms of monomers through oligomer decomposition; Scheme S3: General •OH oxidation mechanism; Schemes S4 and S5: Formation mechanisms of OS and non-OS oxidation products (PDF)

■ AUTHOR INFORMATION

Corresponding Authors

Andrew P. Ault − *Department of Chemistry, College of Literature Sciences and the Arts, University of Michigan, Ann Arbor, Michigan 48109, United States;* orcid.org/0000-0002-7313-8559; Email: aulta@umich.edu

Jason D. Surratt − *Department of Environmental Sciences and Engineering, Gillings School of Global Public Health, University of North Carolina at Chapel Hill, Chapel Hill, North Carolina 27514, United States; Department of Chemistry, College of Arts and Sciences, University of North Carolina at Chapel Hill, Chapel Hill, North Carolina 27599, United States;* orcid.org/0000-0002-6833-1450; Email: surratt@unc.edu

Authors

Jin Yan − *Department of Environmental Sciences and Engineering, Gillings School of Global Public Health, University of North Carolina at Chapel Hill, Chapel Hill, North Carolina 27514, United States*

Yue Zhang − *Department of Environmental Sciences and Engineering, Gillings School of Global Public Health, University of North Carolina at Chapel Hill, Chapel Hill, North Carolina 27514, United States; Aerodyne Research Inc., Billerica, Massachusetts 01821, United States;* Present Address: Department of Atmospheric Sciences, Texas A&M University, College Station, Texas 77843, United States

Yuzhi Chen − *Department of Environmental Sciences and Engineering, Gillings School of Global Public Health, University of North Carolina at Chapel Hill, Chapel Hill, North Carolina 27514, United States;* Present

Address: Atmospheric Sciences and Global Change Division, Pacific Northwest National Laboratory, Richland, Washington 99352, United States.; orcid.org/0000-0002-2547-8428

N. Cazimir Armstrong − *Department of Environmental Sciences and Engineering, Gillings School of Global Public Health, University of North Carolina at Chapel Hill, Chapel Hill, North Carolina 27514, United States*

Nicolas A. Buchenau − *Department of Environmental Sciences and Engineering, Gillings School of Global Public Health, University of North Carolina at Chapel Hill, Chapel Hill, North Carolina 27514, United States*

Ziying Lei − *Department of Environmental Health Sciences, School of Public Health, University of Michigan, Ann Arbor, Michigan 48109, United States;* Present Address: Department of Atmospheric Sciences, Texas A&M University, College Station, Texas 77843, United States

Yao Xiao − *Department of Chemistry, College of Literature Sciences and the Arts, University of Michigan, Ann Arbor, Michigan 48109, United States;* orcid.org/0000-0003-3661-2845

Zhenfa Zhang − *Department of Environmental Sciences and Engineering, Gillings School of Global Public Health, University of North Carolina at Chapel Hill, Chapel Hill, North Carolina 27514, United States*

Andrew T. Lambe − *Aerodyne Research Inc., Billerica, Massachusetts 01821, United States;* orcid.org/0000-0003-3031-701X

Man Nin Chan − *Earth System Science Programme, Faculty of Science, The Chinese University of Hong Kong, Hong Kong 100872, China;* orcid.org/0000-0002-2384-2695

Barbara J. Turpin − *Department of Environmental Sciences and Engineering, Gillings School of Global Public Health, University of North Carolina at Chapel Hill, Chapel Hill, North Carolina 27514, United States;* orcid.org/0000-0003-4513-4187

Avram Gold − *Department of Environmental Sciences and Engineering, Gillings School of Global Public Health, University of North Carolina at Chapel Hill, Chapel Hill, North Carolina 27514, United States;* orcid.org/0000-0003-1383-6635

Complete contact information is available at: https://pubs.acs.org/10.1021/acsearthspacechem.3c00073

Funding

This work was supported by the National Science Foundation under Grants AGS-1703535 (Surratt), AGS-2001027 (Gold, Zhang), and AGS-2039788 (Surratt) as well as CHE-1654149 (Ault), AGS-1703019 (Ault), and AGS-2040610 (Ault). Y.Z. acknowledges support from an NSF Postdoctoral Fellowship (AGS-1524731). In addition, N.A.B. was funded in part by the National Institute for Occupational Safety and Health (Grant No. T42-OH008673), and N.C.A. was funded by the William Neal Reynolds Fellowship of the Royster Society of Fellows at the University of North Carolina at Chapel Hill.

Notes

The authors declare no competing financial interest.

■ ACKNOWLEDGMENTS

The authors would like to thank Drs. Cristine M. D. Machado, Erickson O. dos Santos, and Scot T. Martin for providing the $PM_{2.5}$ sample collected from Manaus, Brazil, Central Amazonia; Philip Croteau and Manjula Canagaratna from Aerodyne, Inc., for providing support for the ACSM instrument and data analysis. We also would like to thank the UNC Center for Galápagos Studies for support of the measurements collected in the Galápagos. AFM was performed at the Scanning Probe Microscopy facility in the Department of Chemistry at the University of Michigan. HILIC/(−)ESI-HR-QTOFMS work was performed in the UNC Biomarker Mass Spectrometry Facility, which is supported by the National Institute of Environmental Health Sciences (grant no. P30ES010126).

■ ABBREVIATIONS

VOC, volatile organic compound; NO, nitric oxide; $^{\bullet}OH$, hydroxyl radical; ISOPOOH, isoprene hydroxyhydroperoxide; IEPOX, isoprene epoxydiol; SOA, secondary organic aerosol; $PM_{2.5}$, fine particulate matter; IEPOX-SOA, isoprene epoxydiol-derived secondary organic aerosol; 2-MTs, 2-methyltetrols; MTSs, methyltetrol sulfates; OS, organosulfate; SE US, southeastern United States; OFR, oxidation flow reactor; PMF, positive matrix factorization; RH, relative humidity; AAS, acidified ammonium sulfate; ACSM, aerosol chemical speciation monitor; SEMS, scanning electrical mobility spectrometer; HILIC/(−)ESI-HR-QTOFMS, hydrophilic interaction liquid chromatography interfaced to electrospray ionization high-resolution quadrupole time-of-flight mass spectrometry operated in the negative ion mode; EIC, extracted ion chromatogram; AFM, atomic force microscopy; PTIR, photothermal infrared spectroscopy; CE, collection efficiency; RIE, relative; ionization efficiency; AMS, aerosol mass spectrometer; OOA, oxidized organic aerosol; VSFS, vibrational sum frequency spectroscopy; GMD, geometric mean diameter

■ REFERENCES

(1) Guenther, A.; Karl, T.; Harley, P.; Wiedinmyer, C.; Palmer, P. I.; Geron, C. Edinburgh Research Explorer Estimates of Global Terrestrial Isoprene Emissions Using MEGAN (Model of Emissions of Gases and Aerosols from Nature) and Physics Estimates of Global Terrestrial Isoprene Emissions Using MEGAN (Model of Emissions of Gases An. *Atmospheric Chem. Phys.* **2006**, *6* (11), 3181−3210.

(2) Guenther, A. B.; Jiang, X.; Heald, C. L.; Sakulyanontvittaya, T.; Duhl, T.; Emmons, L. K.; Wang, X. The Model of Emissions of Gases and Aerosols from Nature Version 2.1 (MEGAN2.1): An Extended and Updated Framework for Modeling Biogenic Emissions. *Geosci. Model Dev.* **2012**, *5* (6), 1471−1492.

(3) Wiedinmyer, C.; Guenther, A.; Harley, P.; Hewitt, N.; Geron, C.; Artaxo, P.; Steinbrecher, R.; Rasmussen, R. Global Organic Emissions from Vegetation. In *Emissions of Atmospheric Trace Compounds*; Advances in Global Change Research; Granier, C., Artaxo, P., Reeves, C. E., Eds.; Beniston, M., Series Ed.; Springer Netherlands: Dordrecht, 2004; Vol. *18*, pp 115−170; DOI: 10.1007/978-1-4020-2167-1_4.

(4) Wiedinmyer, C.; Tie, X.; Guenther, A.; Neilson, R.; Granier, C. Future Changes in Biogenic Isoprene Emissions: How Might They Affect Regional and Global Atmospheric Chemistry? *Earth Interact.* **2006**, *10* (3), 1−19.

(5) Rosenstiel, T. N.; Potosnak, M. J.; Griffin, K. L.; Fall, R.; Monson, R. K. Increased CO2 Uncouples Growth from Isoprene Emission in an Agriforest Ecosystem. *Nature* **2003**, *421* (6920), 256−259.

(6) Pegoraro, E.; Rey, A.; Barron-Gafford, G.; Monson, R.; Malhi, Y.; Murthy, R. The Interacting Effects of Elevated Atmospheric CO2

Concentration, Drought and Leaf-to-Air Vapour Pressure Deficit on Ecosystem Isoprene Fluxes. *Oecologia* **2005**, *146* (1), 120−129.
(7) Fini, A.; Brunetti, C.; Loreto, F.; Centritto, M.; Ferrini, F.; Tattini, M. Isoprene Responses and Functions in Plants Challenged by Environmental Pressures Associated to Climate Change. *Front. Plant Sci.* **2017**, *8*, 1281.
(8) Krechmer, J. E.; Coggon, M. M.; Massoli, P.; Nguyen, T. B.; Crounse, J. D.; Hu, W.; Day, D. A.; Tyndall, G. S.; Henze, D. K.; Rivera-Rios, J. C.; Nowak, J. B.; Kimmel, J. R.; Mauldin, R. L.; Stark, H.; Jayne, J. T.; Sipilä, M.; Junninen, H.; St. Clair, J. M.; Zhang, X.; Feiner, P. A.; Zhang, L.; Miller, D. O.; Brune, W. H.; Keutsch, F. N.; Wennberg, P. O.; Seinfeld, J. H.; Worsnop, D. R.; Jimenez, J. L.; Canagaratna, M. R. Formation of Low Volatility Organic Compounds and Secondary Organic Aerosol from Isoprene Hydroxyhydroperoxide Low-NO Oxidation. *Environ. Sci. Technol.* **2015**, *49* (17), 10330−10339.
(9) D'Ambro, E. L.; Møller, K. H.; Lopez-Hilfiker, F. D.; Schobesberger, S.; Liu, J.; Shilling, J. E.; Lee, B. H.; Kjaergaard, H. G.; Thornton, J. A. Isomerization of Second-Generation Isoprene Peroxy Radicals: Epoxide Formation and Implications for Secondary Organic Aerosol Yields. *Environ. Sci. Technol.* **2017**, *51* (9), 4978−4987.
(10) Paulot, F.; Crounse, J. D.; Kjaergaard, H. G.; Kürten, A.; St. Clair, J. M.; Seinfeld, J. H.; Wennberg, P. O. Unexpected Epoxide Formation in the Gas-Phase Photooxidation of Isoprene. *Science* **2009**, *325* (5941), 730−733.
(11) Surratt, J. D.; Kroll, J. H.; Kleindienst, T. E.; Edney, E. O.; Claeys, M.; Sorooshian, A.; Ng, N. L.; Offenberg, J. H.; Lewandowski, M.; Jaoui, M.; Flagan, R. C.; Seinfeld, J. H. Evidence for Organosulfates in Secondary Organic Aerosol. *Environ. Sci. Technol.* **2007**, *41* (2), 517−527.
(12) Surratt, J. D.; Lewandowski, M.; Offenberg, J. H.; Jaoui, M.; Kleindienst, T. E.; Edney, E. O.; Seinfeld, J. H. Effect of Acidity on Secondary Organic Aerosol Formation from Isoprene. *Environ. Sci. Technol.* **2007**, *41* (15), 5363−5369.
(13) Surratt, J. D.; Chan, A. W. H.; Eddingsaas, N. C.; Chan, M.; Loza, C. L.; Kwan, A. J.; Hersey, S. P.; Flagan, R. C.; Wennberg, P. O.; Seinfeld, J. H. Reactive Intermediates Revealed in Secondary Organic Aerosol Formation from Isoprene. *Proc. Natl. Acad. Sci. U. S. A.* **2010**, *107* (15), 6640−6645.
(14) Lin, Y. H.; Zhang, Z.; Docherty, K. S.; Zhang, H.; Budisulistiorini, S. H.; Rubitschun, C. L.; Shaw, S. L.; Knipping, E. M.; Edgerton, E. S.; Kleindienst, T. E.; Gold, A.; Surratt, J. D. Isoprene Epoxydiols as Precursors to Secondary Organic Aerosol Formation: Acid-Catalyzed Reactive Uptake Studies with Authentic Compounds. *Environ. Sci. Technol.* **2012**, *46* (1), 250−258.
(15) Riva, M.; Chen, Y.; Zhang, Y.; Lei, Z.; Olson, N. E.; Boyer, H. C.; Narayan, S.; Yee, L. D.; Green, H. S.; Cui, T.; Zhang, Z.; Baumann, K.; Fort, M.; Edgerton, E.; Budisulistiorini, S. H.; Rose, C. A.; Ribeiro, I. O.; e Oliveira, R. L.; dos Santos, E. O.; Machado, C. M. D.; Szopa, S.; Zhao, Y.; Alves, E. G.; de Sá, S. S.; Hu, W.; Knipping, E. M.; Shaw, S. L.; Duvoisin Junior, S.; de Souza, R. A. F.; Palm, B. B.; Jimenez, J.-L.; Glasius, M.; Goldstein, A. H.; Pye, H. O. T.; Gold, A.; Turpin, B. J.; Vizuete, W.; Martin, S. T.; Thornton, J. A.; Dutcher, C. S.; Ault, A. P.; Surratt, J. D. Increasing Isoprene Epoxydiol-to-Inorganic Sulfate Aerosol Ratio Results in Extensive Conversion of Inorganic Sulfate to Organosulfur Forms: Implications for Aerosol Physicochemical Properties. *Environ. Sci. Technol.* **2019**, *53* (15), 8682−8694.
(16) Budisulistiorini, S. H.; Nenes, A.; Carlton, A. G.; Surratt, J. D.; McNeill, V. F.; Pye, H. O. T. Simulating Aqueous-Phase Isoprene-Epoxydiol (IEPOX) Secondary Organic Aerosol Production during the 2013 Southern Oxidant and Aerosol Study (SOAS). *Environ. Sci. Technol.* **2017**, *51* (9), 5026−5034.
(17) Chan, M. N.; Surratt, J. D.; Claeys, M.; Edgerton, E. S.; Tanner, R. L.; Shaw, S. L.; Zheng, M.; Knipping, E. M.; Eddingsaas, N. C.; Wennberg, P. O.; Seinfeld, J. H. Characterization and Quantification of Isoprene-Derived Epoxydiols in Ambient Aerosol in the Southeastern United States. *Environ. Sci. Technol.* **2010**, *44* (12), 4590−4596.
(18) Claeys, M.; Graham, B.; Vas, G.; Wang, W.; Vermeylen, R.; Pashynska, V.; Cafmeyer, J.; Guyon, P.; Andreae, M. O.; Artaxo, P.; Maenhaut, W. Formation of Secondary Organic Aerosols Through Photooxidation of Isoprene. *Science* **2004**, *303* (5661), 1173−1176.
(19) Wang, W.; Kourtchev, I.; Graham, B.; Cafmeyer, J.; Maenhaut, W.; Claeys, M. Characterization of Oxygenated Derivatives of Isoprene Related to 2-Methyltetrols in Amazonian Aerosols Using Trimethylsilylation and Gas Chromatography/Ion Trap Mass Spectrometry. *Rapid Commun. Mass Spectrom.* **2005**, *19* (10), 1343−1351.
(20) Lin, Y. H.; Budisulistiorini, S. H.; Chu, K.; Siejack, R. A.; Zhang, H.; Riva, M.; Zhang, Z.; Gold, A.; Kautzman, K. E.; Surratt, J. D. Light-Absorbing Oligomer Formation in Secondary Organic Aerosol from Reactive Uptake of Isoprene Epoxydiols. *Environ. Sci. Technol.* **2014**, *48* (20), 12012−12021.
(21) Frauenheim, M.; Offenberg, J.; Zhang, Z.; Surratt, J. D.; Gold, A. The C_5 − Alkene Triol Conundrum: Structural Characterization and Quantitation of Isoprene-Derived $C_5H_{10}O_3$ Reactive Uptake Products. *Environ. Sci. Technol. Lett.* **2022**, *9* (10), 829−836.
(22) Hu, W. W.; Campuzano-Jost, P.; Palm, B. B.; Day, D. A.; Ortega, A. M.; Hayes, P. L.; Krechmer, J. E.; Chen, Q.; Kuwata, M.; Liu, Y. J.; de Sá, S. S.; McKinney, K.; Martin, S. T.; Hu, M.; Budisulistiorini, S. H.; Riva, M.; Surratt, J. D.; St. Clair, J. M.; Isaacman-Van Wertz, G.; Yee, L. D.; Goldstein, A. H.; Carbone, S.; Brito, J.; Artaxo, P.; de Gouw, J. A.; Koss, A.; Wisthaler, A.; Mikoviny, T.; Karl, T.; Kaser, L.; Jud, W.; Hansel, A.; Docherty, K. S.; Alexander, M. L.; Robinson, N. H.; Coe, H.; Allan, J. D.; Canagaratna, M. R.; Paulot, F.; Jimenez, J. L. Characterization of a Real-Time Tracer for Isoprene Epoxydiols-Derived Secondary Organic Aerosol (IEPOX-SOA) from Aerosol Mass Spectrometer Measurements. *Atmospheric Chem. Phys.* **2015**, *15* (20), 11807−11833.
(23) Hettiyadura, A. P. S.; Al-Naiema, I. M.; Hughes, D. D.; Fang, T.; Stone, E. A. Organosulfates in Atlanta, Georgia: Anthropogenic Influences on Biogenic Secondary Organic Aerosol Formation. *Atmospheric Chem. Phys.* **2019**, *19* (5), 3191−3206.
(24) Glasius, M.; Bering, M. S.; Yee, L. D.; de Sá, S. S.; Isaacman-VanWertz, G.; Wernis, R. A.; Barbosa, H. M. J.; Alexander, M. L.; Palm, B. B.; Hu, W.; Campuzano-Jost, P.; Day, D. A.; Jimenez, J. L.; Shrivastava, M.; Martin, S. T.; Goldstein, A. H. Organosulfates in Aerosols Downwind of an Urban Region in Central Amazon. *Environ. Sci. Process. Impacts* **2018**, *20* (11), 1546−1558.
(25) Hughes, D. D.; Stone, E. A. Organosulfates in the Midwestern United States: Abundance, Composition and Stability. *Environ. Chem.* **2019**, *16* (5), 312.
(26) Hatch, L. E.; Creamean, J. M.; Ault, A. P.; Surratt, J. D.; Chan, M. N.; Seinfeld, J. H.; Edgerton, E. S.; Su, Y.; Prather, K. A. Measurements of Isoprene-Derived Organosulfates in Ambient Aerosols by Aerosol Time-of-Flight Mass Spectrometry - Part 1: Single Particle Atmospheric Observations in Atlanta. *Environ. Sci. Technol.* **2011**, *45* (12), 5105−5111.
(27) Zhang, Y.; Chen, Y.; Lei, Z.; Olson, N. E.; Riva, M.; Koss, A. R.; Zhang, Z.; Gold, A.; Jayne, J. T.; Worsnop, D. R.; Onasch, T. B.; Kroll, J. H.; Turpin, B. J.; Ault, A. P.; Surratt, J. D. Joint Impacts of Acidity and Viscosity on the Formation of Secondary Organic Aerosol from Isoprene Epoxydiols (IEPOX) in Phase Separated Particles. *ACS Earth Space Chem.* **2019**, *3* (12), 2646−2658.
(28) Dubois, C.; Cholleton, D.; Gemayel, R.; Chen, Y.; Surratt, J. D.; George, C.; Rairoux, P.; Miffre, A.; Riva, M. Decrease in Sulfate Aerosol Light Backscattering by Reactive Uptake of Isoprene Epoxydiols. *Phys. Chem. Chem. Phys.* **2021**, *23*, 5927−5935.
(29) Eaves, L. A.; Smeester, L.; Hartwell, H. J.; Lin, Y.-H.; Arashiro, M.; Zhang, Z.; Gold, A.; Surratt, J. D.; Fry, R. C. Isoprene-Derived Secondary Organic Aerosol Induces the Expression of MicroRNAs Associated with Inflammatory/Oxidative Stress Response in Lung Cells. *Chem. Res. Toxicol.* **2020**, *33* (2), 381−387.
(30) Arashiro, M.; Lin, Y.-H.; Zhang, Z.; Sexton, K. G.; Gold, A.; Jaspers, I.; Fry, R. C.; Surratt, J. D. Effect of Secondary Organic

Aerosol from Isoprene-Derived Hydroxyhydroperoxides on the Expression of Oxidative Stress Response Genes in Human Bronchial Epithelial Cells. *Environ. Sci. Process. Impacts* **2018**, *20* (2), 332−339.
(31) Surratt, J. D.; Lin, Y.-H.; Arashiro, M.; Vizuete, W. G.; Zhang, Z.; Gold, A.; Jaspers, I.; Fry, R. C. Understanding the Early Biological Effects of Isoprene-Derived Particulate Matter Enhanced by Anthropogenic Pollutants. *Res. Rep. Health Eff. Inst.* **2019**, No. 198, 1−54.
(32) Chen, Y.; Zhang, Y.; Lambe, A. T.; Xu, R.; Lei, Z.; Olson, N. E.; Zhang, Z.; Szalkowski, T.; Cui, T.; Vizuete, W.; Gold, A.; Turpin, B. J.; Ault, A. P.; Chan, M. N.; Surratt, J. D. Heterogeneous Hydroxyl Radical Oxidation of Isoprene-Epoxydiol-Derived Methyltetrol Sulfates: Plausible Formation Mechanisms of Previously Unexplained Organosulfates in Ambient Fine Aerosols. *Environ. Sci. Technol. Lett.* **2020**, *7* (7), 460−468.
(33) Lam, H. K.; Kwong, K. C.; Poon, H. Y.; Davies, J. F.; Zhang, Z.; Gold, A.; Surratt, J. D.; Chan, M. N. Heterogeneous OH Oxidation of Isoprene-Epoxydiol-Derived Organosulfates: Kinetics, Chemistry and Formation of Inorganic Sulfate. *Atmospheric Chem. Phys.* **2019**, *19* (4), 2433−2440.
(34) Hu, W.; Palm, B. B.; Day, D. A.; Campuzano-Jost, P.; Krechmer, J. E.; Peng, Z.; de Sa, S. S.; Martin, S. T.; Alexander, M. L.; Baumann, K.; Hacker, L.; Kiendler-Scharr, A.; Koss, A. R.; de Gouw, J. A.; Goldstein, A. H.; Seco, R.; Sjostedt, S. J.; Park, J.-H.; Guenther, A. B.; Kim, S.; Canonaco, F.; Prevot, A. S. H.; Brune, W. H.; Jimenez, J. L. Volatility and Lifetime against OH Heterogeneous Reaction of Ambient Isoprene-Epoxydiols-Derived Secondary Organic Aerosol (IEPOX-SOA. *Atmospheric Chem. Phys.* **2016**, *16* (18), 11563−11580.
(35) Armstrong, N. C.; Chen, Y.; Cui, T.; Zhang, Y.; Christensen, C.; Zhang, Z.; Turpin, B. J.; Chan, M. N.; Gold, A.; Ault, A. P.; Surratt, J. D. Isoprene Epoxydiol-Derived Sulfated and Nonsulfated Oligomers Suppress Particulate Mass Loss during Oxidative Aging of Secondary Organic Aerosol. *Environ. Sci. Technol.* **2022**, *56* (23), 16611−16620.
(36) Olson, N. E.; Lei, Z.; Craig, R. L.; Zhang, Y.; Chen, Y.; Lambe, A. T.; Zhang, Z.; Gold, A.; Surratt, J. D.; Ault, A. P. Reactive Uptake of Isoprene Epoxydiols Increases the Viscosity of the Core of Phase-Separated Aerosol Particles. *ACS Earth Space Chem.* **2019**, *3* (8), 1402−1414.
(37) Shiraiwa, M.; Ammann, M.; Koop, T.; Pöschl, U. Gas Uptake and Chemical Aging of Semisolid Organic Aerosol Particles. *Proc. Natl. Acad. Sci. U. S. A.* **2011**, *108* (27), 11003−11008.
(38) Lee, L.; Wilson, K. The Reactive−Diffusive Length of OH and Ozone in Model Organic Aerosols. *J. Phys. Chem. A* **2016**, *120* (34), 6800−6812.
(39) Marais, E. A.; Jacob, D. J.; Jimenez, J. L.; Campuzano-Jost, P.; Day, D. A.; Hu, W.; Krechmer, J.; Zhu, L.; Kim, P. S.; Miller, C. C.; Fisher, J. A.; Travis, K.; Yu, K.; Hanisco, T. F.; Wolfe, G. M.; Arkinson, H. L.; Pye, H. O. T.; Froyd, K. D.; Liao, J.; McNeill, V. F. Aqueous-Phase Mechanism for Secondary Organic Aerosol Formation from Isoprene: Application to the Southeast United States and Co-Benefit of SO2 Emission Controls. *Atmospheric Chem. Phys.* **2016**, *16* (3), 1603−1618.
(40) Pye, H. O. T.; Pinder, R. W.; Piletic, I. R.; Xie, Y.; Capps, S. L.; Lin, Y.-H.; Surratt, J. D.; Zhang, Z.; Gold, A.; Luecken, D. J.; Hutzell, W. T.; Jaoui, M.; Offenberg, J. H.; Kleindienst, T. E.; Lewandowski, M.; Edney, E. O. Epoxide Pathways Improve Model Predictions of Isoprene Markers and Reveal Key Role of Acidity in Aerosol Formation. *Environ. Sci. Technol.* **2013**, *47* (19), 11056−11064.
(41) Jo, D. S.; Hodzic, A.; Emmons, L. K.; Tilmes, S.; Schwantes, R. H.; Mills, M. J.; Campuzano-Jost, P.; Hu, W.; Zaveri, R. A.; Easter, R. C.; Singh, B.; Lu, Z.; Schulz, C.; Schneider, J.; Shilling, J. E.; Wisthaler, A.; Jimenez, J. L. Future Changes in Isoprene-Epoxydiol-Derived Secondary Organic Aerosol (IEPOX SOA) under the Shared Socioeconomic Pathways: The Importance of Physicochemical Dependency. *Atmospheric Chem. Phys.* **2021**, *21* (5), 3395−3425.
(42) Pratt, K. A.; Fiddler, M. N.; Shepson, P. B.; Carlton, A. G.; Surratt, J. D. Organosulfates in Cloud Water above the Ozarks' Isoprene Source Region. *Atmos. Environ.* **2013**, *77*, 231−238.
(43) Boone, E. J.; Laskin, A.; Laskin, J.; Wirth, C.; Shepson, P. B.; Stirm, B. H.; Pratt, K. A. Aqueous Processing of Atmospheric Organic Particles in Cloud Water Collected via Aircraft Sampling. *Environ. Sci. Technol.* **2015**, *49* (14), 8523−8530.
(44) Wolf, M. J.; Zhang, Y.; Zawadowicz, M. A.; Goodell, M.; Froyd, K.; Freney, E.; Sellegri, K.; Rösch, M.; Cui, T.; Winter, M.; Lacher, L.; Axisa, D.; DeMott, P. J.; Levin, E. J. T.; Gute, E.; Abbatt, J.; Koss, A.; Kroll, J. H.; Surratt, J. D.; Cziczo, D. J. A Biogenic Secondary Organic Aerosol Source of Cirrus Ice Nucleating Particles. *Nat. Commun.* **2020**, *11* (1), 4834.
(45) Spolnik, G.; Wach, P.; Rudziński, K. J.; Szmigielski, R.; Danikiewicz, W. Tracing the Biogenic Secondary Organic Aerosol Markers in Rain, Snow and Hail. *Chemosphere* **2020**, *251*, No. 126439.
(46) Guo, H.; Xu, L.; Bougiatioti, A.; Cerully, K. M.; Capps, S. L.; Hite, J. R.; Carlton, A. G.; Lee, S.-H.; Bergin, M. H.; Ng, N. L.; Nenes, A.; Weber, R. J. Fine-Particle Water and PH in the Southeastern United States. *Atmospheric Chem. Phys.* **2015**, *15* (9), 5211−5228.
(47) Bates, K. H.; Crounse, J. D.; St. Clair, J. M.; Bennett, N. B.; Nguyen, T. B.; Seinfeld, J. H.; Stoltz, B. M.; Wennberg, P. O. Gas Phase Production and Loss of Isoprene Epoxydiols. *J. Phys. Chem. A* **2014**, *118* (7), 1237−1246.
(48) Zhang, Z.; Lin, Y.-H.; Zhang, H.; Surratt, J. D.; Ball, L. M.; Gold, A. Technical Note: Synthesis of Isoprene Atmospheric Oxidation Products: Isomeric Epoxydiols and the Rearrangement Products Cis- and Trans-3-Methyl-3,4-Dihydroxytetrahydrofuran. *Atmospheric Chem. Phys.* **2012**, *12* (18), 8529−8535.
(49) Lambe, A. T.; Ahern, A. T.; Williams, L. R.; Slowik, J. G.; Wong, J. P. S.; Abbatt, J. P. D.; Brune, W. H.; Ng, N. L.; Wright, J. P.; Croasdale, D. R.; Worsnop, D. R.; Davidovits, P.; Onasch, T. B. Characterization of Aerosol Photooxidation Flow Reactors: Heterogeneous Oxidation, Secondary Organic Aerosol Formation and Cloud Condensation Nuclei Activity Measurements. *Atmospheric Meas. Technol.* **2011**, *4* (3), 445−461.
(50) Li, R.; Palm, B. B.; Ortega, A. M.; Hlywiak, J.; Hu, W.; Peng, Z.; Day, D. A.; Knote, C.; Brune, W. H.; de Gouw, J. A.; Jimenez, J. L. Modeling the Radical Chemistry in an Oxidation Flow Reactor: Radical Formation and Recycling, Sensitivities, and the OH Exposure Estimation Equation. *J. Phys. Chem. A* **2015**, *119* (19), 4418−4432.
(51) Rowe, J. P.; Lambe, A. T.; Brune, W. H. Technical Note: Effect of Varying the λ = 185 and 254 Nm Photon Flux Ratio on Radical Generation in Oxidation Flow Reactors. *Atmospheric Chem. Phys.* **2020**, *20* (21), 13417−13424.
(52) Mao, J.; Ren, X.; Brune, W. H.; Olson, J. R.; Crawford, J. H.; Fried, A.; Huey, L. G.; Cohen, R. C.; Heikes, B.; Singh, H. B.; Blake, D. R.; Sachse, G. W.; Diskin, G. S.; Hall, S. R.; Shetter, R. E. Airborne Measurement of OH Reactivity during INTEX-B. *Atmospheric Chem. Phys.* **2009**, *9* (1), 163−173.
(53) Cui, T.; Zeng, Z.; dos Santos, E. O.; Zhang, Z.; Chen, Y.; Zhang, Y.; Rose, C. A.; Budisulistiorini, S. H.; Collins, L. B.; Bodnar, W. M.; de Souza, R. A. F.; Martin, S. T.; Machado, C. M. D.; Turpin, B. J.; Gold, A.; Ault, A. P.; Surratt, J. D. Development of a Hydrophilic Interaction Liquid Chromatography (HILIC) Method for the Chemical Characterization of Water-Soluble Isoprene Epoxydiol (IEPOX)-Derived Secondary Organic Aerosol. *Environ. Sci. Process. Impacts* **2018**, *20* (11), 1524−1536.
(54) Dazzi, A.; Prater, C. B.; Hu, Q.; Chase, D. B.; Rabolt, J. F.; Marcott, C. AFM−IR: Combining Atomic Force Microscopy and Infrared Spectroscopy for Nanoscale Chemical Characterization. *Appl. Spectrosc.* **2012**, *66* (12), 1365−1384.
(55) Ault, A. P. Aerosol Acidity: Novel Measurements and Implications for Atmospheric Chemistry. *Acc. Chem. Res.* **2020**, *53* (9), 1703−1714.
(56) Alfarra, M. R.; Coe, H.; Allan, J. D.; Bower, K. N.; Boudries, H.; Canagaratna, M. R.; Jimenez, J. L.; Jayne, J. T.; Garforth, A. A.; Li, S.-M.; Worsnop, D. R. Characterization of Urban and Rural Organic Particulate in the Lower Fraser Valley Using Two Aerodyne Aerosol Mass Spectrometers. *Atmos. Environ.* **2004**, *38* (34), 5745−5758.
(57) Duplissy, J.; DeCarlo, P. F.; Dommen, J.; Alfarra, M. R.; Metzger, A.; Barmpadimos, I.; Prevot, A. S. H.; Weingartner, E.;

https://doi.org/10.1021/acsearthspacechem.3c00073
ACS Earth Space Chem. 2023, 7, 1916−1928

Tritscher, T.; Gysel, M.; Aiken, A. C.; Jimenez, J. L.; Canagaratna, M. R.; Worsnop, D. R.; Collins, D. R.; Tomlinson, J.; Baltensperger, U. Relating Hygroscopicity and Composition of Organic Aerosol Particulate Matter. *Atmospheric Chem. Phys.* **2011**, *11* (3), 1155−1165.
(58) Mei, F.; Setyan, A.; Zhang, Q.; Wang, J. CCN Activity of Organic Aerosols Observed Downwind of Urban Emissions during CARES. *Atmospheric Chem. Phys.* **2013**, *13* (24), 12155−12169.
(59) Ng, N. L.; Canagaratna, M. R.; Jimenez, J. L.; Chhabra, P. S.; Seinfeld, J. H.; Worsnop, D. R. Changes in Organic Aerosol Composition with Aging Inferred from Aerosol Mass Spectra. *Atmospheric Chem. Phys.* **2011**, *11* (13), 6465−6474.
(60) Liu, J.; Alexander, L.; Fast, J. D.; Lindenmaier, R.; Shilling, J. E. Aerosol Characteristics at the Southern Great Plains Site during the HI-SCALE Campaign. *Atmospheric Chem. Phys.* **2021**, *21* (6), 5101−5116.
(61) Ng, N. L.; Canagaratna, M. R.; Zhang, Q.; Jimenez, J. L.; Tian, J.; Ulbrich, I. M.; Kroll, J. H.; Docherty, K. S.; Chhabra, P. S.; Bahreini, R.; Murphy, S. M.; Seinfeld, J. H.; Hildebrandt, L.; Donahue, N. M.; DeCarlo, P. F.; Lanz, V. A.; Prévôt, A. S. H.; Dinar, E.; Rudich, Y.; Worsnop, D. R. Organic Aerosol Components Observed in Northern Hemispheric Datasets from Aerosol Mass Spectrometry. *Atmospheric Chem. Phys.* **2010**, *10* (10), 4625−4641.
(62) Smith, J. D.; Kroll, J. H.; Cappa, C. D.; Che, D. L.; Liu, C. L.; Ahmed, M.; Leone, S. R.; Worsnop, D. R.; Wilson, K. R. The Heterogeneous Reaction of Hydroxyl Radicals with Sub-Micron Squalane Particles: A Model System for Understanding the Oxidative Aging of Ambient Aerosols. *Atmos. Chem. Phys.* **2009**, *9*, 3209.
(63) Riva, M.; Bell, D. M.; Hansen, A.-M. K.; Drozd, G. T.; Zhang, Z.; Gold, A.; Imre, D.; Surratt, J. D.; Glasius, M.; Zelenyuk, A. Effect of Organic Coatings, Humidity and Aerosol Acidity on Multiphase Chemistry of Isoprene Epoxydiols. *Environ. Sci. Technol.* **2016**, *50* (11), 5580−5588.
(64) Kessler, S. H.; Smith, J. D.; Che, D. L.; Worsnop, D. R.; Wilson, K. R.; Kroll, J. H. Chemical Sinks of Organic Aerosol: Kinetics and Products of the Heterogeneous Oxidation of Erythritol and Levoglucosan. *Environ. Sci. Technol.* **2010**, *44* (18), 7005−7010.
(65) Slade, J. H.; Knopf, D. A. Multiphase OH Oxidation Kinetics of Organic Aerosol: The Role of Particle Phase State and Relative Humidity. *Geophys. Res. Lett.* **2014**, *41* (14), 5297−5306.
(66) Kessler, S. H.; Nah, T.; Daumit, K. E.; Smith, J. D.; Leone, S. R.; Kolb, C. E.; Worsnop, D. R.; Wilson, K. R.; Kroll, J. H. OH-Initiated Heterogeneous Aging of Highly Oxidized Organic Aerosol. *J. Phys. Chem. A* **2012**, *116* (24), 6358−6365.
(67) Chan, M. N.; Zhang, H.; Goldstein, A. H.; Wilson, K. R. Role of Water and Phase in the Heterogeneous Oxidation of Solid and Aqueous Succinic Acid Aerosol by Hydroxyl Radicals. *J. Phys. Chem. C* **2014**, *118* (50), 28978−28992.
(68) Baars, H.; Ansmann, A.; Althausen, D.; Engelmann, R.; Heese, B.; Müller, D.; Artaxo, P.; Paixao, M.; Pauliquevis, T.; Souza, R. Aerosol Profiling with Lidar in the Amazon Basin during the Wet and Dry Season: AEROSOL PROFILING IN AMAZONIA. *J. Geophys. Res. Atmospheres* **2012**, *117* (D21), 1.
(69) Liu, Y.; Seco, R.; Kim, S.; Guenther, A. B.; Goldstein, A. H.; Keutsch, F. N.; Springston, S. R.; Watson, T. B.; Artaxo, P.; Souza, R. A. F.; McKinney, K. A.; Martin, S. T. Isoprene Photo-Oxidation Products Quantify the Effect of Pollution on Hydroxyl Radicals over Amazonia. *Sci. Adv.* **2018**, *4* (4), 1−9.
(70) Ortega, A. M.; Hayes, P. L.; Peng, Z.; Palm, B. B.; Hu, W.; Day, D. A.; Li, R.; Cubison, M. J.; Brune, W. H.; Graus, M.; Warneke, C.; Gilman, J. B.; Kuster, W. C.; de Gouw, J.; Gutiérrez-Montes, C.; Jimenez, J. L. Real-Time Measurements of Secondary Organic Aerosol Formation and Aging from Ambient Air in an Oxidation Flow Reactor in the Los Angeles Area. *Atmospheric Chem. Phys.* **2016**, *16* (11), 7411−7433.
(71) Warneke, C. Comparison of Daytime and Nighttime Oxidation of Biogenic and Anthropogenic VOCs along the New England Coast in Summer during New England Air Quality Study 2002. *J. Geophys. Res.* **2004**, *109* (D10), No. D10309.
(72) Lu, K. D.; Rohrer, F.; Holland, F.; Fuchs, H.; Bohn, B.; Brauers, T.; Chang, C. C.; Häseler, R.; Hu, M.; Kita, K.; Kondo, Y.; Li, X.; Lou, S. R.; Nehr, S.; Shao, M.; Zeng, L. M.; Wahner, A.; Zhang, Y. H.; Hofzumahaus, A. Observation and Modelling of OH and HO2 Concentrations in the Pearl River Delta 2006: A Missing OH Source in a VOC Rich Atmosphere. *Atmospheric Chem. Phys.* **2012**, *12* (3), 1541−1569.
(73) Lu, K. D.; Hofzumahaus, A.; Holland, F.; Bohn, B.; Brauers, T.; Fuchs, H.; Hu, M.; Häseler, R.; Kita, K.; Kondo, Y.; Li, X.; Lou, S. R.; Oebel, A.; Shao, M.; Zeng, L. M.; Wahner, A.; Zhu, T.; Zhang, Y. H.; Rohrer, F. Missing OH Source in a Suburban Environment near Beijing: Observed and Modelled OH and HO2 Concentrations in Summer 2006. *Atmospheric Chem. Phys.* **2013**, *13* (2), 1057−1080.
(74) Liu, H.; Jacob, D. J.; Bey, I.; Yantosca, R. M. Constraints from ^{210}Pb and ^{7}Be on Wet Deposition and Transport in a Global Three-Dimensional Chemical Tracer Model Driven by Assimilated Meteorological Fields. *J. Geophys. Res. Atmospheres* **2001**, *106* (D11), 12109−12128.
(75) Kristiansen, N. I.; Stohl, A.; Olivié, D. J. L.; Croft, B.; Søvde, O. A.; Klein, H.; Christoudias, T.; Kunkel, D.; Leadbetter, S. J.; Lee, Y. H.; Zhang, K.; Tsigaridis, K.; Bergman, T.; Evangeliou, N.; Wang, H.; Ma, P.-L.; Easter, R. C.; Rasch, P. J.; Liu, X.; Pitari, G.; Di Genova, G.; Zhao, S. Y.; Balkanski, Y.; Bauer, S. E.; Faluvegi, G. S.; Kokkola, H.; Martin, R. V.; Pierce, J. R.; Schulz, M.; Shindell, D.; Tost, H.; Zhang, H. Evaluation of Observed and Modelled Aerosol Lifetimes Using Radioactive Tracers of Opportunity and an Ensemble of 19 Global Models. *Atmospheric Chem. Phys.* **2016**, *16* (5), 3525−3561.
(76) Zhao, R.; Aljawhary, D.; Lee, A. K. Y.; Abbatt, J. P. D. Rapid Aqueous-Phase Photooxidation of Dimers in the α-Pinene Secondary Organic Aerosol. *Environ. Sci. Technol. Lett.* **2017**, *4* (6), 205−210.
(77) Gordon, B. P.; Moore, F. G.; Scatena, L. F.; Richmond, G. L. On the Rise: Experimental and Computational Vibrational Sum Frequency Spectroscopy Studies of Pyruvic Acid and Its Surface-Active Oligomer Species at the Air−Water Interface. *J. Phys. Chem. A* **2019**, *123* (49), 10609−10619.
(78) Lim, C. Y.; Browne, E. C.; Sugrue, R. A.; Kroll, J. H. Rapid Heterogeneous Oxidation of Organic Coatings on Submicron Aerosols. *Geophys. Res. Lett.* **2017**, *44* (6), 2949−2957.
(79) Kirpes, R. M.; Lei, Z.; Fraund, M.; Gunsch, M. J.; May, N. W.; Barrett, T. E.; Moffett, C. E.; Schauer, A. J.; Alexander, B.; Upchurch, L. M.; China, S.; Quinn, P. K.; Moffet, R. C.; Laskin, A.; Sheesley, R. J.; Pratt, K. A.; Ault, A. P. Solid Organic-Coated Ammonium Sulfate Particles at High Relative Humidity in the Summertime Arctic Atmosphere. *Proc. Natl. Acad. Sci. U. S. A.* **2022**, *119* (14), No. e2104496119.
(80) Lei, Z.; Olson, N. E.; Zhang, Y.; Chen, Y.; Lambe, A. T.; Zhang, J.; White, N. J.; Atkin, J. M.; Banaszak Holl, M. M.; Zhang, Z.; Gold, A.; Surratt, J. D.; Ault, A. P. Morphology and Viscosity Changes after Reactive Uptake of Isoprene Epoxydiols in Submicrometer Phase Separated Particles with Secondary Organic Aerosol Formed from Different Volatile Organic Compounds. *ACS Earth Space Chem.* **2022**, *6* (4), 871−882.
(81) Lei, Z.; Chen, Y.; Zhang, Y.; Cooke, M. E.; Ledsky, I. R.; Armstrong, N. C.; Olson, N. E.; Zhang, Z.; Gold, A.; Surratt, J. D.; Ault, A. P. Initial PH Governs Secondary Organic Aerosol Phase State and Morphology after Uptake of Isoprene Epoxydiols (IEPOX). *Environ. Sci. Technol.* **2022**, *56* (15), 10596−10607.
(82) Bondy, A. L.; Kirpes, R. M.; Merzel, R. L.; Pratt, K. A.; Banaszak Holl, M. M.; Ault, A. P. Atomic Force Microscopy-Infrared Spectroscopy of Individual Atmospheric Aerosol Particles: Subdiffraction Limit Vibrational Spectroscopy and Morphological Analysis. *Anal. Chem.* **2017**, *89* (17), 8594−8598.
(83) Olson, N. E.; Xiao, Y.; Lei, Z.; Ault, A. P. Simultaneous Optical Photothermal Infrared (O-PTIR) and Raman Spectroscopy of Submicrometer Atmospheric Particles. *Anal. Chem.* **2020**, *92* (14), 9932−9939.
(84) Comuñas, M. J. P.; Paredes, X.; Gaciño, F. M.; Fernández, J.; Bazile, J. P.; Boned, C.; Daridon, J. L.; Galliero, G.; Pauly, J.; Harris, K. R.; Assael, M. J.; Mylona, S. K. Reference Correlation of the

Viscosity of Squalane from 273 to 373 K at 0.1 MPa. *J. Phys. Chem. Ref. Data* **2013**, *42* (3), No. 033101.
(85) Russell, G. A. Deuterium-Isotope Effects in the Autoxidation of Aralkyl Hydrocarbons. Mechanism of the Interaction of PEroxy Radicals [1]. *J. Am. Chem. Soc.* **1957**, *79* (14), 3871−3877.
(86) Bennett, J. E.; Summers, R. Product Studies of the Mutual Termination Reactions of *Sec* -Alkylperoxy Radicals: Evidence for Non-Cyclic Termination. *Can. J. Chem.* **1974**, *52* (8), 1377−1379.
(87) Stevens, P.; L'Esperance, D.; Chuong, B.; Martin, G. Measurements of the Kinetics of the OH-Initiated Oxidation of Isoprene: Radical Propagation in the OH + Isoprene + O2 + NO Reaction System. *Int. J. Chem. Kinet.* **1999**, *31* (9), 637−643.
(88) Salamone, M.; Bietti, M. Reaction Pathways of Alkoxyl Radicals. The Role of Solvent Effects on C−C Bond Fragmentation and Hydrogen Atom Transfer Reactions. *Synlett* **2014**, *25* (13), 1803−1816.
(89) Čeković, Ž. Reactions of δ-Carbon Radicals Generated by 1,5-Hydrogen Transfer to Alkoxyl Radicals. *Tetrahedron* **2003**, *59* (41), 8073−8090.
(90) Cope, J. D.; Abellar, K. A.; Bates, K. H.; Fu, X.; Nguyen, T. B. Aqueous Photochemistry of 2-Methyltetrol and Erythritol as Sources of Formic Acid and Acetic Acid in the Atmosphere. *ACS Earth Space Chem.* **2021**, *5* (6), 1265−1277.
(91) Wach, P.; Spólnik, G.; Surratt, J. D.; Blaziak, K.; Rudzinski, K. J.; Lin, Y.-H.; Maenhaut, W.; Danikiewicz, W.; Claeys, M.; Szmigielski, R. Structural Characterization of Lactone-Containing MW 212 Organosulfates Originating from Isoprene Oxidation in Ambient Fine Aerosol. *Environ. Sci. Technol.* **2020**, *54* (3), 1415−1424.
(92) Wennberg, P. O.; Bates, K. H.; Crounse, J. D.; Dodson, L. G.; McVay, R. C.; Mertens, L. A.; Nguyen, T. B.; Praske, E.; Schwantes, R. H.; Smarte, M. D.; St Clair, J. M.; Teng, A. P.; Zhang, X.; Seinfeld, J. H. Gas-Phase Reactions of Isoprene and Its Major Oxidation Products. *Chem. Rev.* **2018**, *118* (7), 3337−3390.
(93) Shiraiwa, M.; Li, Y., Sr.; Tsimpidi, A.; Karydis, V.; Berkemeier, T.; Pandis, S. N.; Lelieveld, J.; Koop, T.; Poeschl, U. Global Distribution of Secondary Organic Aerosol Particle Phase State. *Nat. Commun.* **2017**, *8*, 15002.
(94) Song, M.; Marcolli, C.; Krieger, U. K.; Zuend, A.; Peter, T. Liquid-Liquid Phase Separation in Aerosol Particles: Dependence on O:C, Organic Functionalities, and Compositional Complexity: PHASE SEPARATION. *Geophys. Res. Lett.* **2012**, *39* (19), 1.
(95) Petters, S. S.; Pagonis, D.; Claflin, M. S.; Levin, E. J. T.; Petters, M. D.; Ziemann, P. J.; Kreidenweis, S. M. Hygroscopicity of Organic Compounds as a Function of Carbon Chain Length and Carboxyl, Hydroperoxy, and Carbonyl Functional Groups. *J. Phys. Chem. A* **2017**, *121* (27), 5164−5174.
(96) Docherty, K. S.; Corse, E. W.; Jaoui, M.; Offenberg, J. H.; Kleindienst, T. E.; Krug, J. D.; Riedel, T. P.; Lewandowski, M. Trends in the Oxidation and Relative Volatility of Chamber-Generated Secondary Organic Aerosol. *Aerosol Sci. Technol.* **2018**, *52* (9), 992−1004.
(97) Zuend, A.; Seinfeld, J. H. Modeling the Gas-Particle Partitioning of Secondary Organic Aerosol: The Importance of Liquid-Liquid Phase Separation. *Atmospheric Chem. Phys.* **2012**, *12* (9), 3857−3882.
(98) O'Dowd, C. D., Wagner, P., Eds. *Nucleation and Atmospheric Aerosols: 17th International Conference, Galway, Ireland, 2007*; Springer: Dordrecht; London, 2007.
(99) Zhang, Y.; Nichman, L.; Spencer, P.; Jung, J. I.; Lee, A.; Heffernan, B. K.; Gold, A.; Zhang, Z.; Chen, Y.; Canagaratna, M. R.; Jayne, J. T.; Worsnop, D. R.; Onasch, T. B.; Surratt, J. D.; Chandler, D.; Davidovits, P.; Kolb, C. E. The Cooling Rate- and Volatility-Dependent Glass-Forming Properties of Organic Aerosols Measured by Broadband Dielectric Spectroscopy. *Environ. Sci. Technol.* **2019**, *53* (21), 12366−12378.
(100) Kristensen, K.; Watne, Å. K.; Hammes, J.; Lutz, A.; Petäjä, T.; Hallquist, M.; Bilde, M.; Glasius, M. High-Molecular Weight Dimer Esters Are Major Products in Aerosols from α-Pinene Ozonolysis and the Boreal Forest. *Environ. Sci. Technol. Lett.* **2016**, *3* (8), 280−285.
(101) Kourtchev, I.; Fuller, S. J.; Giorio, C.; Healy, R. M.; Wilson, E.; O'Connor, I.; Wenger, J. C.; McLeod, M.; Aalto, J.; Ruuskanen, T. M.; Maenhaut, W.; Jones, R.; Venables, D. S.; Sodeau, J. R.; Kulmala, M.; Kalberer, M. Molecular Composition of Biogenic Secondary Organic Aerosols Using Ultrahigh-Resolution Mass Spectrometry: Comparing Laboratory and Field Studies. *Atmospheric Chem. Phys.* **2014**, *14* (4), 2155−2167.
(102) Quéléver, L. L. J.; Kristensen, K.; Normann Jensen, L.; Rosati, B.; Teiwes, R.; Daellenbach, K. R.; Peräkylä, O.; Roldin, P.; Bossi, R.; Pedersen, H. B.; Glasius, M.; Bilde, M.; Ehn, M. Effect of Temperature on the Formation of Highly Oxygenated Organic Molecules (HOMs) from Alpha-Pinene Ozonolysis. *Atmospheric Chem. Phys.* **2019**, *19* (11), 7609−7625.
(103) Gao, S.; Ng, N. L.; Keywood, M.; Varutbangkul, V.; Bahreini, R.; Nenes, A.; He, J.; Yoo, K. Y.; Beauchamp, J. L.; Hodyss, R. P.; Flagan, R. C.; Seinfeld, J. H. Particle Phase Acidity and Oligomer Formation in Secondary Organic Aerosol. *Environ. Sci. Technol.* **2004**, *38* (24), 6582−6589.
(104) Jonsson, Å. M.; Hallquist, M.; Ljungström, E. Impact of Humidity on the Ozone Initiated Oxidation of Limonene, Δ [3] -Carene, and α-Pinene. *Environ. Sci. Technol.* **2006**, *40* (1), 188−194.

https://doi.org/10.1021/acsearthspacechem.3c00073
ACS Earth Space Chem. 2023, 7, 1916−1928